Fall 11-1996

NMR studies of acyl chain-protein interactions

Mark Christian Oswood
Yale University.

Abstract
NMR Studies of Acyl Chain-Protein Interactions
Mark Christian Oswood
1996

An approach employing heteronuclear NMR is presented for monitoring the interactions between long-chain fatty acids and proteins which are involved in their synthesis and intracellular transport. Two naturally occurring fatty acids, hexadecanoic (palmitic) and cis-9-10-methylene-hexadecanoic (MHA) acids were labeled using a biosynthetic scheme with ^{13}C acetate as a source. The biosynthetic incorporation of ^{13}C from a two carbon source resulted in sequential pairs of ^{13}C atoms in the product. When combined with double-quantum spectroscopy, a highly efficient suppression of natural abundance background resonances results. Proton-detected two and three-dimensional experiments which correlate double-quantum carbon chemical shifts with proton shifts were developed to resolve and assign chemical shifts of the selectively detected cis-9,10-methylene hexadecanoic acid (MHA) and palmitic acid in sodium dodecyl sulfate (SDS) micelles.

A subset of the experiments was applied to a complex between MHA and rat adipocyte lipid binding protein (ALBP), a protein involved in intracellular fatty acid transport. With the use of double-quantum spectroscopy, we were able to selectively observe and assign chemical shifts to all ^{13}C enriched pairs of resonances in the MHA-ALBP complex. Changes in

chemical shifts between micelle and protein-bound states are interpreted in terms of protein-induced conformational preferences for the bound fatty acid. Comparison with x-ray crystallographic data on similar protein-fatty acid complexes suggests that non-linear fatty acid conformations observed in the crystal structure are preserved when the complex is examined in solution.

Similar double quantum experiments were successfully applied to palmitic acid covalently coupled to *Escherichia coli* acyl carrier protein (ACP), a protein cofactor in fatty acid synthesis. Carbon-13 chemical shifts were once again used to analyze the conformation of the acyl chain. The chain was found to have an increase in gauche character at several positions, suggesting a bent conformation in the bound state. In addition, ^{13}C filtered cross-relaxation experiments were conducted. Cross relaxation data localized the methyl terminus of the acyl chain to a binding pocket in ACP consisting of phenylalanine-50, tyrosine-71 and isoleucine-72. These data are interpreted using the known structure of octanoyl-ACP and previous models for acyl chain binding to suggest that the thioester bond may protrude from the protein complex as the chain is lengthened in order to facilitate enzyme catalyzed reactions necessary for fatty acid synthesis.

NMR Studies of Acyl Chain-Protein Interactions

A Dissertation
Presented to the Faculty of the Graduate School
of
Yale University
in Candidacy for the Degree of
Doctor of Philosophy

by
Mark Christian Oswood

Dissertation Director: James H. Prestegard

November 1996

For
Ann
and
Christian

Acknowledgements

Many thanks are due to Dr. James Prestegard, without whom none of this work would have been possible. He is a knowledgeable, patient, and dedicated teacher. In addition, he has been very understanding in scheduling my studies at Yale Medical School.

Thanks are also due to Drs. Gary Brudvig and Don Crothers for their helpful suggestions as members of my dissertation committee.

Many current and past members of the Prestegard laboratory have contributed to this work. In particular Michael Andrec, Joel Tolman, and Drs. John Chung, Blake Hill, and Anne Horvath have contributed valuable technical assistance and informative discussions. They and Jeanne Weaver, Judit Losonczi, Andrew Fowler, Eric Sayers, Kai Huang, Ronnie Ghose, and Drs. Kitty Howard, Brian Salvatore, Brian Hare, Yves Aubin, and Frode Rise also contributed helpful discussions.

We thank Drs. Leonard Banaszak and Judith LaLonde for supplying *E. coli* JM101 containing the ALBP plasmid, Dr. John Cronan, Jr. for supplying *E. coli* LCD25, and Dr. Charles Rock for supplying the acyl-ACP synthetase expression system.

Many previous teachers were sources of encouragement and advice, especially Drs. F. G. Prendergast and Gary Miessler.

Many Yale faculty had not heard of St. Olaf College, but former M.D./Ph.D. Program director Dr. Howard Rasmussen accepted me into the program and deserves my appreciation. Thanks also to MaryBeth Brandi for invaluable administrative assistance.

Many times my parents have offered encouragement, even when they did not understand what I was doing or the length of time required to complete the task.

Finally, I must thank Ann and Christian for their love and understanding, without which this would have been impossible.

Table of Contents

List of Figures

List of Tables

Chapter 1: Introduction

Interactions between acyl chains and proteins are important in many areas of biology and medicine. Knowledge of structural and dynamic features of these interactions would be useful in designing compounds to interact with known systems as well as predicting behavior of newly discovered systems. Methods commonly used for the study of lipid-protein complexes have limited usefulness. Fluorescence spectroscopy, while highly sensitive, requires the use of unnatural lipids and provides few structural details. X-ray crystallography gives rich structural detail when suitable crystals can be obtained, but little insight is given concerning possible variations in conformation and motion when systems function in solution. A method of study which provides minimal perturbation to the system while giving specific structural and motional information would be useful. The synthesis and characterization of isotopically labeled fatty acid probes was undertaken to address these problems. These probes have been used in high-resolution NMR studies of lipid-protein complexes.

1.1 Significance

Acyl chain-protein interactions are central to many physiological and pathological processes. The absorption and transport of lipid nutrients during

digestion depends on several soluble proteins, including lipases and lipoproteins. Fatty acids are transported intracellularly by soluble fatty acid binding proteins (FABP's). These proteins serve to protect the cell from the harmful detergent effects of high concentrations of free fatty acid, which may reach concentrations of several millimolar in some cells (Clarke & Armstrong, 1989). A variety of these proteins have been discovered in tissues including brain, fat, and liver.

A large number of soluble proteins participate in fatty acid biosynthesis (Slabas & Fawcett, 1992). Some are specialized at carrying the hydrophobic intermediates, such as soluble acyl carrier proteins (ACP's). An interaction between acyl-ACP and a hydrolase enzyme determines the chain length in the final product (Ohlrogge, et al, 1978). An understanding of this interaction could help in efforts to produce crops with different seed oil compositions (Voelker, et al., 1992). The role of ACP's extends beyond de novo synthesis to include such processes as acyl transfer to proteins and lipid modification (Guerra & Browse, 1990).

A variety of disease processes involve fatty acids or their associated proteins. Hemolysin, a toxin secreted by some strains of *Escherichia coli*, requires an ACP-dependent acylation for activation (Issartel, et al., 1991; Stanley, et al., 1994). Gram negative bacteria in the bloodstream produce an often-fatal disease called septic shock, which is caused by an interaction between the glycolipid components of the bacterial cell wall and a white blood

cell surface protein (Schumann, et. al., 1990). In *E. coli*, acyl-ACP is a cofactor for the synthesis of these toxic cell wall components (Brozek & Raetz, 1990). An understanding of acyl chain interactions in these systems could lead to design of inhibitors of septic shock. Thus, the development of methods for the study of acyl chain-protein interactions could have broad implications for studies of basic biosynthesis as well as human disease.

1.2 Background

In this study we focus on acyl chain-protein interactions in two specific systems: rat adipocyte lipid binding protein and *E. coli* acyl carrier protein.

1.2.1 Fatty Acid Binding Proteins

The fatty acid binding protein (FABP) family comprises a group of homologous cytosolic lipid binding proteins involved in intracellular transport of lipids. Members of this family are found distributed in various body organs including intestine, liver, adipose tissue, heart, muscle, and brain (Banaszak, et al., 1994). As much as 60% of the cytosolic fatty acids in cells may be non-covalently bound to these proteins (Spener, et. al., 1989). All of these proteins have a strong primary sequence homology. These proteins also share homology with other lipid carrier proteins, such as retinol and sterol binding proteins (Veerkamp, et. al., 1991).

The crystal structure of the 131-residue rat adipocyte lipid binding protein (ALBP) has been solved and refined to 1.6 Å resolution (Xu, et al., 1993). The protein is composed of two five-stranded beta-sheets and two short alpha-helical segments (see Figure 1.1). The beta-sheets are orthogonally opposed and form a hydrophobic binding pocket for a single hydrophobic ligand. This hydrophobic ligand may be either a long-chain fatty acid or retinoic acid (Matarese & Bernlohr, 1988). In the absence of bound ligand, the central binding pocket is filled with water molecules (Xu, et al., 1993).

Some understanding of the way in which ALBP interacts with a fatty acid can be obtained from the crystal structure. ALBP has polar interactions with fatty acid carboxyl groups through arginine-126 and tyrosine-128 (Xu, et al., 1993). It also has substantial hydrophobic interactions with the remainder of the chain. Even in the presence of bound ligand, several water molecules appear to remain in the binding pocket of ALBP (LaLonde, et al., 1994). This finding suggests variability of the protein-ligand interactions in this system, which may be manifest in comparison of the crystal and solution state. No solution state structural studies have previously been performed on ALBP, so the bound conformation of the ligand and the residues with which it interacts in solution are not known.

1.2.2 Acyl Carrier Protein

One of the proteins involved in fatty acid biosynthesis, *E. coli* ACP, has been extensively investigated in this laboratory. It is a 77 amino acid protein

of molecular weight 8847 g/mol. ACP plays a central role in lipid biosynthesis as it carries the growing chain between the enzymes involved in synthesis. It interacts directly with at least seven other proteins in this role (Slabas & Fawcett, 1992). The lipid is carried between enzymes by covalent attachment to a 4-phosphopantotheine prosthetic group attached to serine-36 of ACP. However, additional hydrophobic interactions with the acyl chain have been postulated, and it is intriguing to speculate that these additional interactions can influence the ultimate course of biosynthesis.

NMR resonances for apo-ACP have been completely assigned (Holak & Prestegard, 1986). These assignments were used in combination with two-dimensional NOE spectra to determine distance constraints for the protein. A structure for apo-ACP was determined using distance geometry methods followed by molecular dynamics refinement of structures (Holak, et. al., 1988). The structure in solution is composed of three alpha-helical segments which are joined by turns lacking a well-defined secondary structure (see Figure 1.2). A cleft containing hydrophobic side chains is seen between the second and third helices, and this cleft was proposed as the binding site for the acyl chain.

NMR studies of acyl chain binding to this cleft in ACP are complicated by the chemical shift degeneracy of resonances assigned to the acyl chain and nearby hydrophobic side chains. The binding of an acyl chain attached to the prosthetic group was first investigated using ^{19}F NMR methods to surmount

this resolution problem (Jones, 1991). Octanoic acid was labeled with ^{19}F at various positions along the chain, giving unique site-specific resonances for observation. These octanoic acid derivatives were then attached to ACP by a chemical synthesis. The structure of acyl-ACP was solved with the use of ^{1}H-^{1}H cross-relaxation data. ^{19}F-^{1}H cross-relaxation studies determined residues which were directly in contact with the fluorines on the acyl chain, and these data were incorporated into the structure. As postulated based on the apoprotein structure, the data were in agreement with a hydrophobic binding pocket between the second and third helices.

These studies, as with all ^{19}F methods, suffered from several limitations. While fluorine is approximately the same size as hydrogen, it has very different electrostatic properties, which could alter its binding mode. In addition, the chemistry of the ^{19}F-labeled lipids is such that it is difficult to synthesize and esterify fatty acids fluorinated at the 2 or 3 positions on the acyl chain. Therefore, vital structural information about this area is missing. An NMR method which used ^{13}C would provide more complete and reliable structural information. Isotopic perturbations on replacement of ^{12}C with ^{13}C are minimal. Structures could also be obtained for longer-chain acyl-ACP's since biosynthetic labeling of longer chains is an option.

1.3 Experimental Approach

Carbon-13 is an NMR active spin $\frac{1}{2}$ isotope with good spectral dispersion. Sensitivity for direct observation is low ($\frac{1}{64}$ of protons; Ernst, et al., 1987), but modern indirect observation methods can largely compensate for this. Fatty acids labeled with ^{13}C will be produced through a biosynthetic pathway and used to provide specific insight into structural interactions with proteins. Because the labeling is isotopic in nature, the lipids have chemical properties identical to natural lipids. Each carbon is in principle spectroscopically unique, and therefore may be individually observed. Furthermore, since only the acyl chain component of the complex to be studied is enriched in ^{13}C, it can be selectively observed. Spectroscopy will be done through the use of indirect methods, which can give a 16-fold increase in sensitivity over direct ^{13}C detection as well as improving resolution (Ernst, et al., 1987). Much can be accomplished through normal ^{13}C chemical shift dispersion; this dispersion will be extended through the use of double-quantum spectroscopy. double-quantum spectroscopy causes adjacent pairs of nuclei to resonate at the sum of their shifts, which simplifies assignment by linking them in the resulting spectra. Pulsed field gradients will be used for coherence selection. These give excellent supression of artifacts common in heteronuclear spectra (Tolman, et al., 1992) without decreasing sensitivity in many experiments (Kay, et al, 1992).

NMR structural studies of biological systems have traditionally been accomplished with the use of NOE's. These cross-relaxation data can be interpreted to provide distance information used in building structural models. While this approach is used in this study, its utility is limited by the poor proton chemical shift dispersion found in long chain fatty acids. Another approach to structure which has recently been followed involves the use of chemical shift data. Chemical shifts are sensitive to changes in torsion angles (de Dios, et al., 1993), and the carbon chemical shift resolution given by the experiments described above can give valuable structural information in systems where NOE's cannot be obtained.

Initial applications will be to fatty acids in SDS micelles. These samples provide a system into which lipids could be introduced in relatively high concentration, eliminating sensitivity concerns from initial method development. Proton and carbon single and double-quantum spectra of palmitic acid and cis-9,10-methylene hexadecanoic acid (MHA) will be collected and fully assigned in this system.

Once the spectroscopic methods for the use of these lipid probes are established, studies will be extended to the rat adipocyte lipid binding protein. ALBP has been cloned and expressed in *E. coli* (Xu, et al., 1991). While its size is within the range of proteins now under study by NMR methods, we were prevented from determining an NMR structure by protein instability in solution. However, the ability to focus on the acyl chain using double-

quantum filtered spectroscopy did allow analysis of the bound conformation of the acyl chain using primarily chemical shift perturbation data. Studies will characterize the binding of a novel ligand and compare this to data gathered on the crystal state.

To further explore the uses of ^{13}C labeled lipids, *E. coli* acyl carrier protein (ACP) will be used. An enzymatic synthesis is used to attach the fatty acids to ACP (Rock & Cronan, 1981). Chemical shift data are again employed to determine the conformation of the acyl chain. In addition, heteronuclear-correlated NOE experiments are performed to determine which protein residues directly contact the acyl chain. A new model for ACP binding of long acyl chains is proposed based on these data.

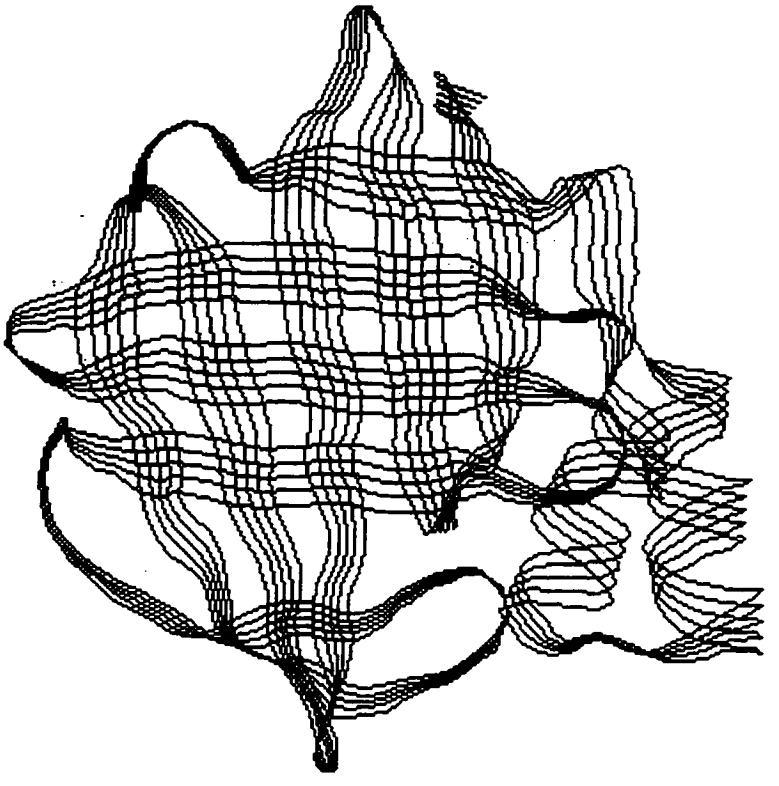

Figure 1.1: Ribbon view of crystal structure of ALBP (Xu, et al., 1993). The beta-sheets are orthogonally opposed with the ligand binding pocket between them. There are two short helices which can be seen at the right side of the figure.

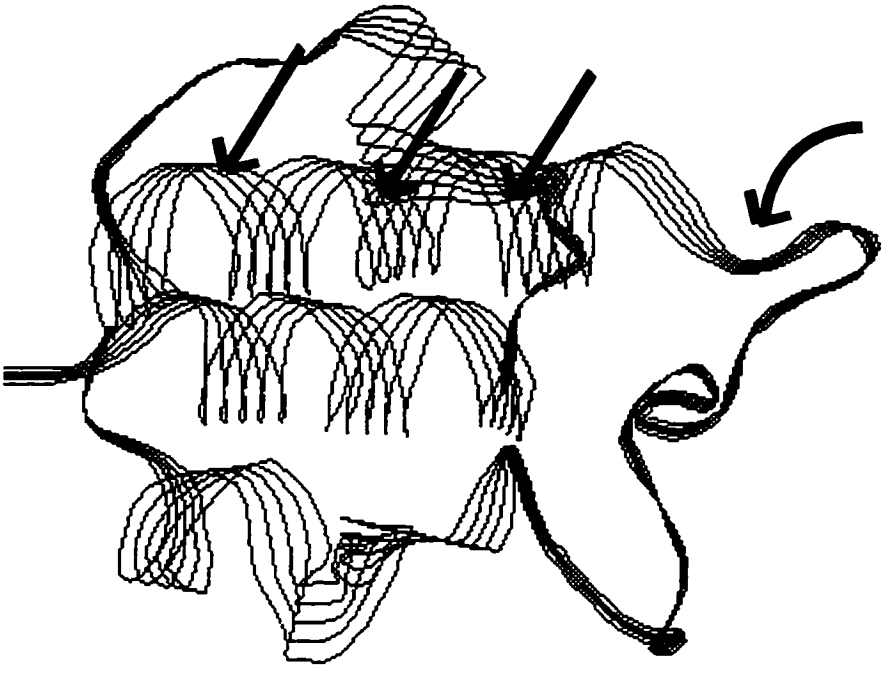

Figure 1.2: Ribbon view of ACP solution structure (Holak, et al., 1988). The protein folds into three parallel helices in solution. The putative acyl chain binding site is indicated with straight arrows. The position of serine-36, which is the site of attachment of the prosthetic group, is indicated with a curved arrow.

Chapter 2: Carbon-13 Labeled Fatty Acids

2.1 Introduction

Several K12 strains of *Escherichia coli* were developed some time ago to aid in the biosynthesis of ^{13}C enriched fatty acids (Cronan & Batchelor, 1973). In particular, *E. coli* LCD25 can specifically and efficiently use acetate as a ^{13}C source in the production of fatty acids (Munford, et al., 1992). LCD25 contains two metabolic mutations which direct exogenous acetate into lipid synthesis (see Figure 2.1). One mutation prevents the organism from producing acetate through glycolysis, and the other blocks metabolism of acetate through the tri-carboxylic acid cycle. Since acetate does not undergo one-carbon metabolism in the bacteria used, the isotopes present in the acetate supplement will be added to the growing acyl chain in a pairwise manner. Carbons derived from the acetate methyl will always be at an even numbered position in the fatty acid, and those derived from the carbonyl will fall in an odd numbered position. The labeling pattern can significantly simplify the analysis of double-quantum spectra which result.

In this study we have made use of hexadecanoic (palmitic) acid and cis-9,10-methylene-hexadecanoic acid (MHA). These are both naturally occurring fatty acids from *E. coli* (Cronan, J.E. Jr., et al., 1974) and are readily produced in useful quantities as the ^{13}C labeled species. Most of the NMR

experimental techniques used with acyl chain-protein samples have been developed on more concentrated samples of these fatty acids in liquid micelles. These micellar samples simulate the aqueous environment of protein solutions while allowing concentrations of 20 mM of ^{13}C enriched fatty acids to minimize sensitivity problems. The primary experiment developed for chemical shift assignment of these lipids is a proton-detected carbon-carbon double-quantum correlation experiment. Complete chemical shift assignment of these fatty acid samples will be important in the conformational analysis to follow.

2.2 Materials & Methods

Carbon-13 labeled fatty acids were produced biosynthetically using *E. coli* LCD25 as described by Munford, et al. (1992). Briefly, bacterial cultures were grown in medium E (Cronan & Batchelor, 1973) supplemented with 33mg ^{13}C enriched sodium acetate per liter, 40 mg D,L-methionine/liter, and 20 mg kanamycin/liter. Double-labeled acetate was used to produce odd-even labeling patterns, while a mixture of equal amounts of C_1 and C_2 single-labeled acetate was used to produce even-odd labeling patterns. Bacteria were grown to an optical density of 0.3 at 550 nm, after which cells were pelleted by centrifugation at 5000 rpm for 10 minutes in a Beckman JA-10 rotor. Lipids were extracted from bacterial pellets using a chloroform-

methanol mixture (Ways & Hanahan, 1964) and saponified by reflux in ethanolic potassium hydroxide. Fatty acid composition and isotopic enrichment were assayed by gas chromatography-mass spectrometry after esterification of small aliquots in methanol-HCl. Free fatty acids were purified by reverse-phase HPLC (Bailie, et al., 1982) in a solvent system of 45: 35: 25: 0.1 water: acetonitrile: tetrahydrofuran: acetic acid on a Waters 19x300 mm C-18 column with detection by refractive index (see figure 2.3). Purity was assayed by NMR spectroscopy and determined to be >95%. Yield for a typical 6 liter growth was 15 mg palmitic acid, which represents incorporation of 19% of added acetate into this species.

Fatty acid NMR samples were prepared by dissolving fatty acid in 3% SDS/20 mM sodium phosphate buffer pH 7.5/D_2O at a concentration of 20 mM or by dissolving in $CDCl_3$ to a concentration of 30 mM. Experiments on SDS samples were conducted at 37°C (MHA) or 50° C (palmitate) to place the lipid mixture into a phase where NMR spectral lines were narrow.

NMR spectroscopy was carried out on a GE Omega 500 spectrometer equipped with a G17 pulsed field gradient accessory capable of generating gradients of 20 G/cm along 3 independent axes. For MHA samples, proton shifts were referenced to water at 4.75 ppm directly. Carbon shifts were referenced indirectly to water by using a frequency ratio of 0.251450200. For palmitic acid samples, proton shifts were referenced to DSS as an internal standard at 0.00 ppm, and carbon shifts were referenced indirectly to DSS as

described by Wishart, et al. (1995). Shifts referenced to water can be converted to the DSS standard by adding 2.5 ppm to carbon shifts and subtracting 0.16 ppm from proton shifts.

Three-dimensional proton-carbon-carbon correlation experiments were done as described by Chung et al. (1993) with two minor modifications. In the original experiment gradient coherence selection was performed twice, first after converting carbon double-quantum coherences to single quantum coherences, and again after converting carbon magnetization to proton magnetization. Here, the second and third carbon gradients were omitted for purposes of increasing sensitivity. A single gradient pulse of relative power 1.0 was applied at the end of the carbon double-quantum evolution period to encode carbon two-quantum coherence, and another gradient pulse of relative power 0.5 was applied immediately before the detection period to decode the coherence which had transferred to protons. This minor modification increases the sensitivity of the experiment twofold while still providing good suppression of artifacts. Also, the sign of the final gradient was alternated between successive t_1 increments to achieve quadrature detection in the indirect dimension (Tolman, et al., 1992). The modified pulse sequence is shown in Figure 2.4. Heteronuclear single quantum correlation experiments were done using the standard enhanced sensitivity experiment of Kay, et al. (1992).

2.3 Results

E. coli LCD25, a biosynthetic mutant (Munford, et al., 1992), was used to prepare palmitic acid enriched in a pairwise fashion. This pairwise enrichment was done in order to aid in the chemical shift assignment of the acyl chain. The labeling pattern produced in fatty acids from cultures grown with double-labeled sodium acetate is depicted in Figure 2.2A. Those pairs which are enriched in ^{13}C are shown with darkened bonds. By dilution with natural abundance acetate during biosynthesis, overall enrichment can be held at less than 30%. In this case, the occurrence of even-odd pairs (e.g. 2-3, 4-5) of ^{13}C isotope is comparatively rare and may be disregarded. We shall refer to this pattern as molecule **Ia**. In molecule **Ia**, odd to even pair connections are easily made, but even to odd pair connections are not. Therefore, we used a second sample with an alternate enrichment scheme. Figure 2.2B shows the labeling pattern which is produced in MHA using a mixture of equal parts of C_1 and C_2 enriched sodium acetate. This resulted in fatty acids with ^{13}C pairs complementary to those found in **Ia**, allowing even-odd connections to be made. The maximum theoretical enrichment at a given single carbon site in this molecule, henceforth called **Ib**, is only 50% because this is the enrichment of the carbon source. Therefore, pairs will be present in 25% abundance at best, as the probability of an even carbon from one acetate being adjacent to an enriched odd carbon from the next acetate is 0.5. The 25% maximum

enrichment limit means decreased sensitivity for experiments involving **Ib** when compared to **Ia**.

The use of two distinct labeling patterns requires the preparation of two samples and the performance of two sets of NMR experiments in order to unambiguously assign the spectra. However, this scheme has the advantage of simplifying the spectra by reducing the number of peaks in each double-quantum spectrum by half. For a molecule such as a long chain fatty acid with extreme chemical shift degeneracy, this simplification far outweighs the inconvenience of dual sample preparation.

2.3.1 cis-9,10-Methylene Hexadecanoic Acid (MHA)

The heteronuclear proton-carbon single quantum correlation (HSQC) spectrum for ^{13}C enriched MHA with even-odd labeling (**Ib**) in SDS is shown in Figure 2.5. This spectrum demonstrates the resolution and background suppression possible through the use of normal single quantum carbon editing. In principle, individual peaks appear for each carbon site. Peaks are clearly resolved and labeled for positions 2,3,9-10,14,15, and 16. The chemical shifts for these positions are listed in Table II-A. Positions 9 and 10 in the cyclopropane ring are degenerate in these spectra. The bridging methylene in a cyclopropane fatty acid is derived from a different carbon source and does not appear in these carbon-edited spectra (Law, 1971). While the resolution is good, resonances for positions 4,5,6,7,8,12,and 13 are still unresolved at approximately 1.3 ppm and 29 ppm in proton and carbon spectra, respectively.

It should also be noted that several natural abundance peaks due to the relatively highly concentrated SDS acyl chains still appear. These natural abundance peaks are easily distinguished from the MHA peaks in the HSQC spectrum **Ia** because the pairwise labeled fatty acids result in peaks with partially resolved J-couplings in the indirect dimension. Natural abundance peaks would appear at greater intensity in protein samples where the expected ratio of nearly degenerate methylene resonances from amino acid sidechains to methylenes from fatty acids is even greater.

The improved resolution needed for complete chemical shift assignment of MHA in SDS was obtained using a three-dimensional correlation experiment developed by Chung, et al. (1994) that utilizes a double-quantum dimension. double-quantum spectroscopy uses the sum of chemical shifts and therefore enhances resolution by adding small differences in shift. By optimizing experimental conditions for the excitation of adjacent ^{13}C nuclei, direct through-bond assignments are easily made. This experiment, shown in Figure 2.4, was originally designed for use with molecules uniformly enriched in ^{13}C to the level of 25%. It begins with proton magnetization, transfers this to directly bound carbons, and allows for carbon evolution. The carbon coherences present are converted to carbon double-quantum coherences for a second evolution period. The J-evolution delays in this experiment are optimized to create double-quantum coherences in directly bound carbons. This selection is possible because carbon one-bond coupling

constants are an order of magnitude larger than two- or three-bond coupling constants. This double-quantum magnetization is converted back to single quantum carbon magnetization and finally transferred to protons for detection. Correlations between adjacent carbons are established by the fact that the double-quantum coherences transfer equally to the individual carbons involved and their attached protons. A carbon-proton plane at a given double-quantum frequency will show autopeaks at each spin pair's proton and carbon frequencies and crosspeaks at the proton and carbon frequency of a scalar coupled adjacent site. The experiment may conveniently be thought of as an HSQC separated into planes by double-quantum frequency with crosspeaks added between adjacent carbon-proton spin pairs. Because of the double-quantum evolution domain, no crosspeaks from natural abundance sites are observed, since pairs of rare ^{13}C nuclei are exceedingly rare (0.01% natural abundance for adjacent pairs).

Assignments conveniently start at the terminal methyl, which can clearly be distinguished in spectra for **Ib** by its lack of a strong carbon-carbon J coupling as well as its characteristic methyl carbon chemical shift of 13.8 ppm. In the three-dimensional spectrum of **Ia**, a connection is clearly made between the methyl spin system and the adjacent methylene, position 15. This connection is made by looking in the three-dimensional spectrum for a peak with the proton and carbon single quantum shifts of position 16. The resonance which falls at the same double-quantum frequency must be

position 15. Once the assignment for position 15 was made, positions 15 and 14 were connected using the spectrum of **Ib**. The assignment continues with positions 14 and 13 in **Ia**, as shown in Figure 2.6. This is a slice of the three-dimensional matrix at the double-quantum shift of the 14-13 pair. Position 13 could not be resolved in the single quantum correlation spectrum (Figure 2.5), but here it is unambiguously assigned with a proton shift of 1.37 ppm and a carbon shift of 29.7 ppm by using the single quantum-double-quantum spectrum. Once the shift at position 13 is determined, the shift for position 12 can be determined by finding the resonance correlated to the resonance for position 13 in the spectrum of **Ib**. This slice of the three-dimensional matrix is shown in Figure 2.7. Here, position 12 may be assigned at shifts of 1.46 ppm in proton and 30.6 ppm in carbon. In this way, assignments may be made for the entire length of the chain. These assignments are given in Table II-A. Along with the assignments are the observed double-quantum shifts and calculated double-quantum shifts based upon the assignments of single quantum frequencies. Small differences may be attributed to second order effects in these highly degenerate systems.

2.3.2 Hexadecanoic (Palmitic) Acid

As expected, complete chemical shift assignment of palmitic acid is even more challenging than that of MHA due to severe chemical shift degeneracy in the mid-portion of the chain. An HSQC spectrum, which correlates carbon chemical shifts with those of directly attached protons, is

shown in Figure 2.8. The resolution is significantly improved over one-dimensional proton spectra, but it is clear that only 5 out of 15 carbon-proton spin systems are well resolved. These positions are labelled in Figure 2.8 and their shifts are tabulated in Table II-B. Positions 4-13 are not resolved and all resonate at about 1.3 ppm in proton and 33 ppm in carbon. Also, several background peaks from SDS are visible in this spectrum. For this reason, carbon double-quantum spectroscopy was applied to this system.

To better resolve chemical shifts, we again performed a three-dimensional proton-carbon single quantum-carbon double-quantum correlation experiment (Chung, et al., 1993; see figure 2.4). By performing this experiment on two samples with alternate labeling patterns, it was straightforward to assign chemical shifts for each position. This process was described in detail for MHA and details will not be presented here. The observed carbon single and double-quantum shifts are reported in Table II-B. In some cases near degeneracy of single quantum carbon chemical shifts led to ambiguities in assignment of double-quantum peaks. For this reason, double-quantum shifts were calculated from the assigned single quantum shifts to confirm the assignment. If the single quantum shifts were incorrectly assigned, we would expect significant deviation from the observed double-quantum shifts at misassigned positions. These calculated shifts are reported in Table II-B and can be seen to match the actual double-quantum shifts quite closely.

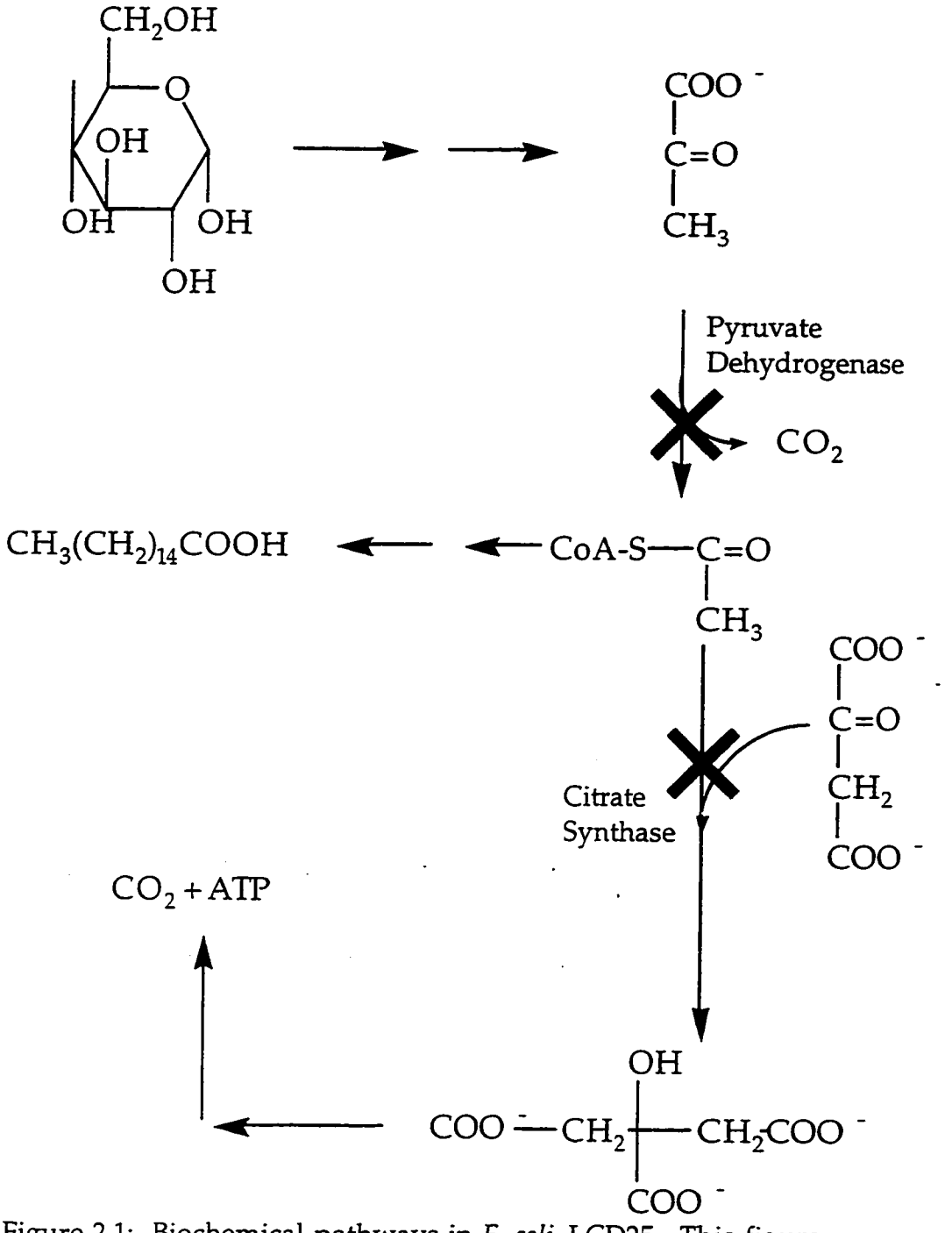

Figure 2.1: Biochemical pathways in *E. coli* LCD25. This figure indicates the principal pathways for acetate metabolism in *E. coli* LCD25. The X's indicate the mutations present in this strain. This strain requires acetate for growth, and nearly all of the acetate is directed into fatty acid synthesis.

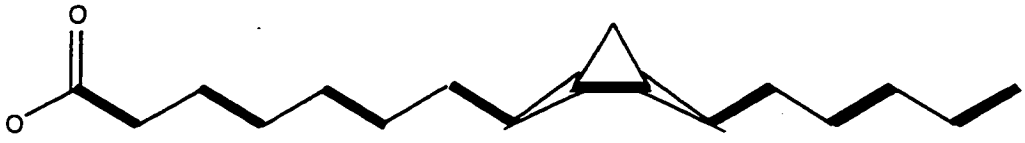

Molecule **Ia**

Molecule **Ib**

Figure 2.2: The two labeling patterns for MHA used in these experiments. **Ia** is referred to as odd-even labeling and **Ib** is referred to as even-odd labeling. Those pairs of atoms which are selectively enriched in ^{13}C are indicated with boldface bonds in each case.

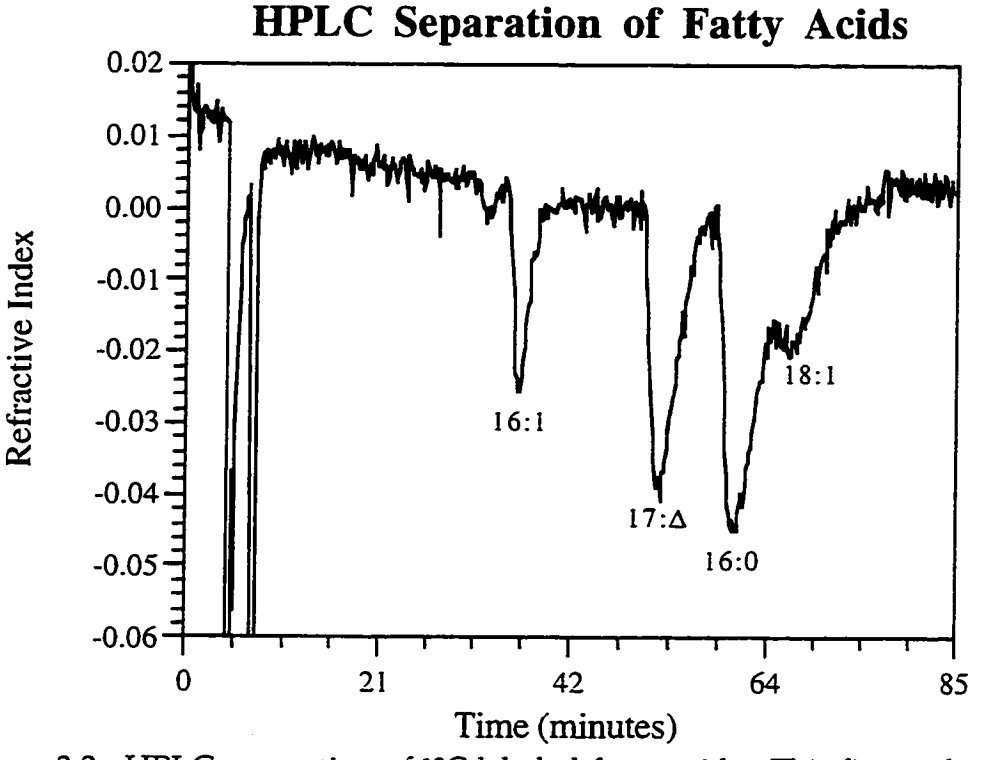

Figure 2.3: HPLC separation of ^{13}C labeled fatty acids. This figure shows the reverse-phase HPLC separation of fatty acids used in this study. The fatty acids were separated on a C-18 column with a water:acetonitrile: tetrahydrofuran solvent system and detected by changes in refractive index.

Heteronuclear Carbon Single Quantum-Double Quantum Correlation Experiment (HSQDQC)

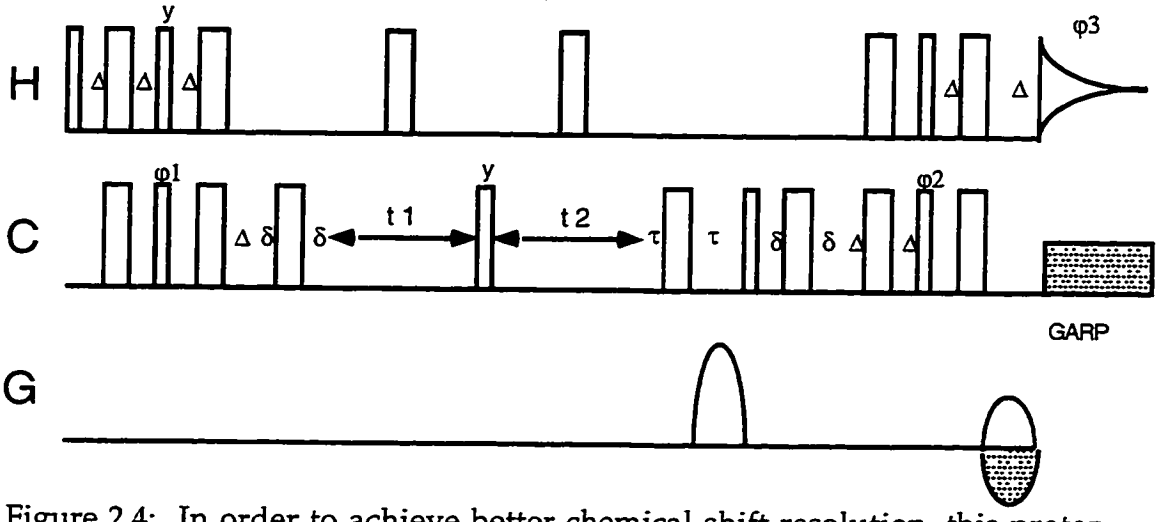

Figure 2.4: In order to achieve better chemical shift resolution, this proton-detected carbon-carbon double-quantum correlation experiment was performed. Carbon single quantum magnetization evolves during t1, and double-quantum magnetization evolves during t2. The gradient pulses select only that magnetization which is transferred from carbon double-quantum coherence to proton. All phases x except as indicated: $\phi1=x+tppi$; $\phi2=\{y,-y\}$; $\phi3=\{x,-x\}$. $\delta=1/(4J_{CC})$, $\Delta=1/(8J_{CH})$, τ=gradient length + ring time. J_{CC} was set at 35 Hz, J_{CH} was set at 125 Hz , and τ was 1.05 ms. This pulse seqeunce is adapted from Chung, et. al. (1993).

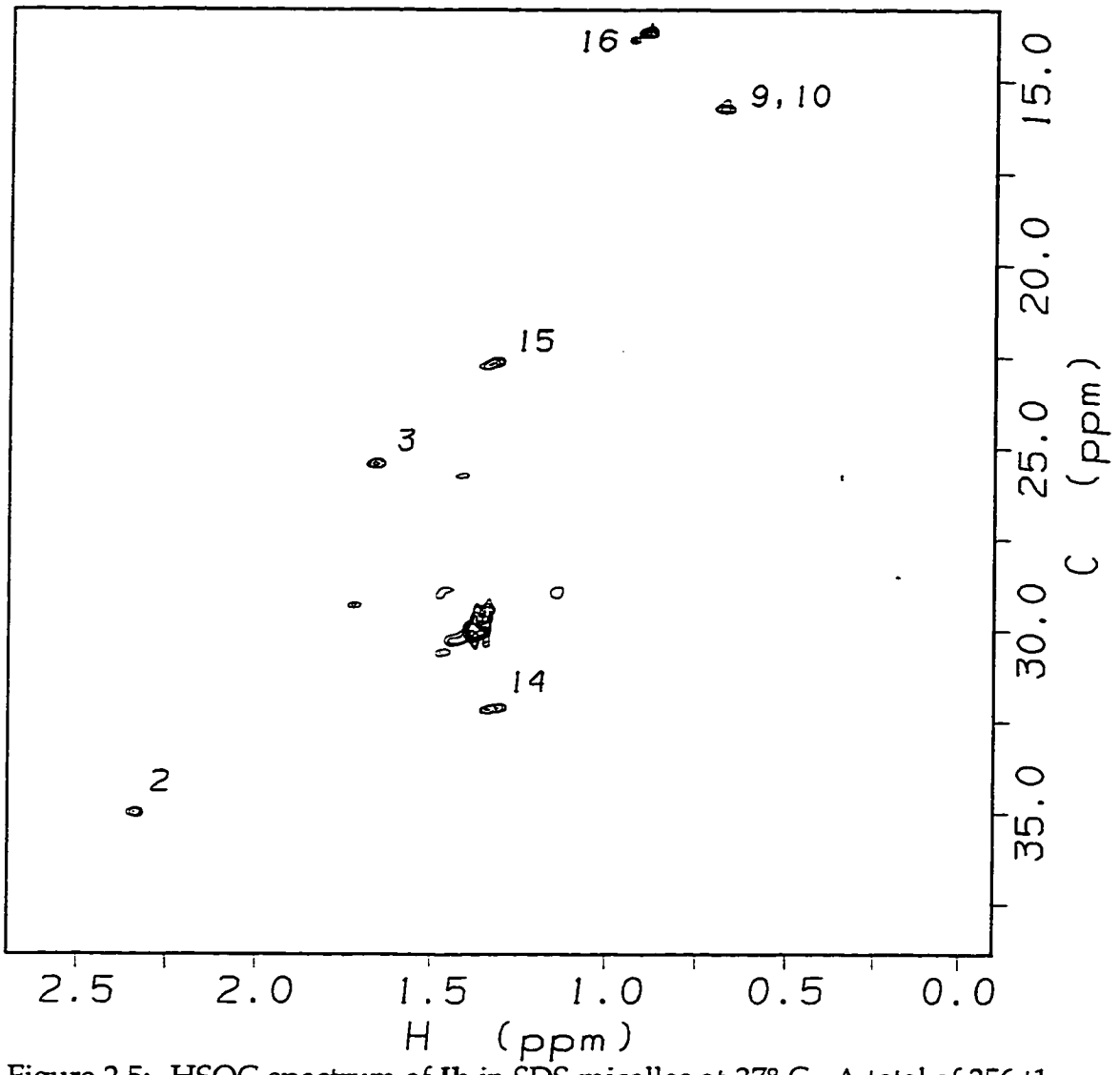

Figure 2.5: HSQC spectrum of **Ib** in SDS micelles at 37° C. A total of 256 t1 points were acquired with an indirect sweep width of 3250 hz. Data were acquired in 30 minutes at 11.7T with a GE Omega 500 spectrometer.

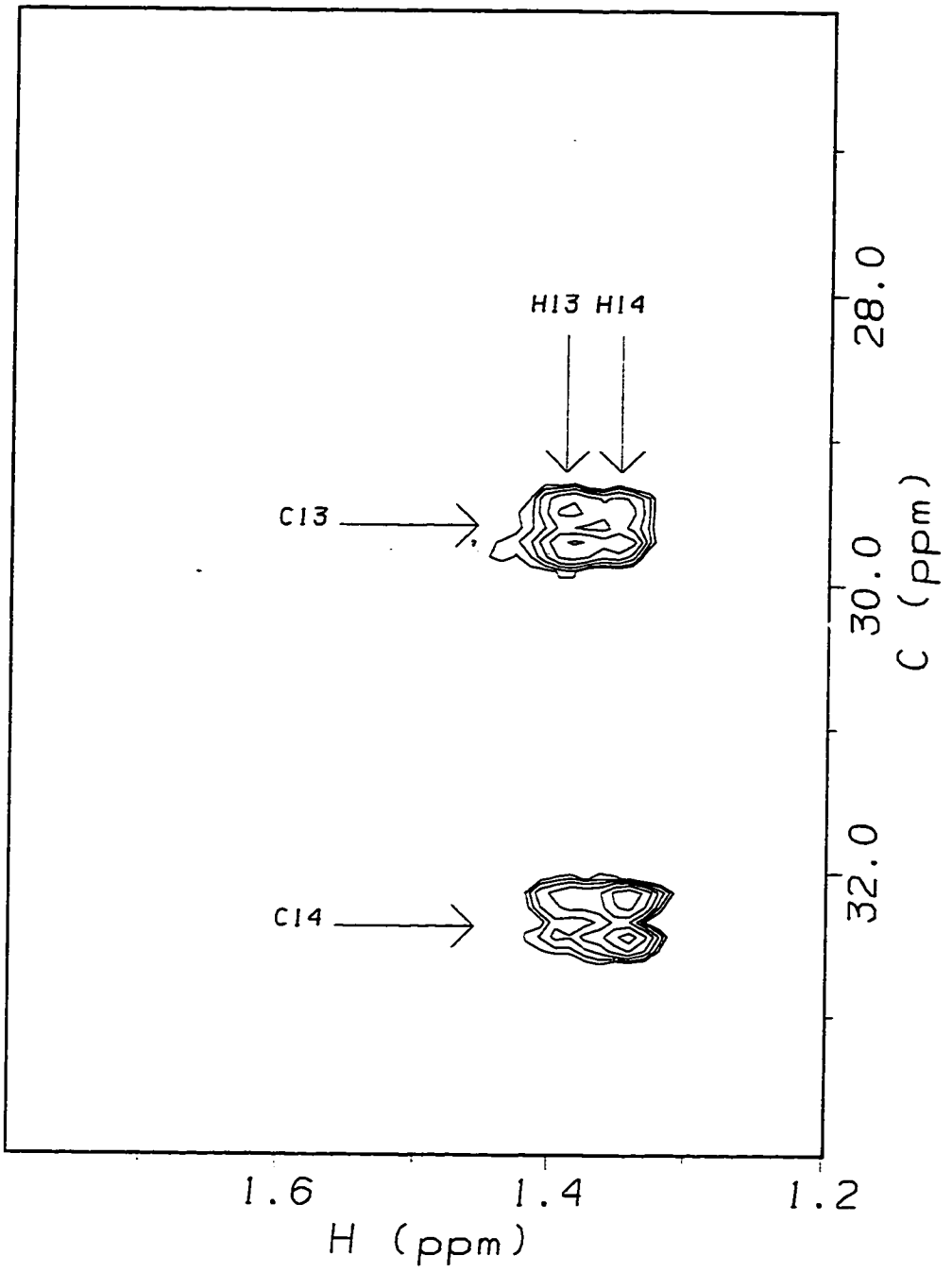

Figure 2.6: Two-dimensional slice of the three-dimensional spectrum of molecule **Ia** in SDS which shows the crosspeaks between positions 13 and 14. 128 t1 (single quantum) and 120 t2 (double-quantum) points were acquired at 11.7T in 11 hours. The t1 and t2 sweep widths were 1625 and 1000 hz centered at 28.5 ppm.

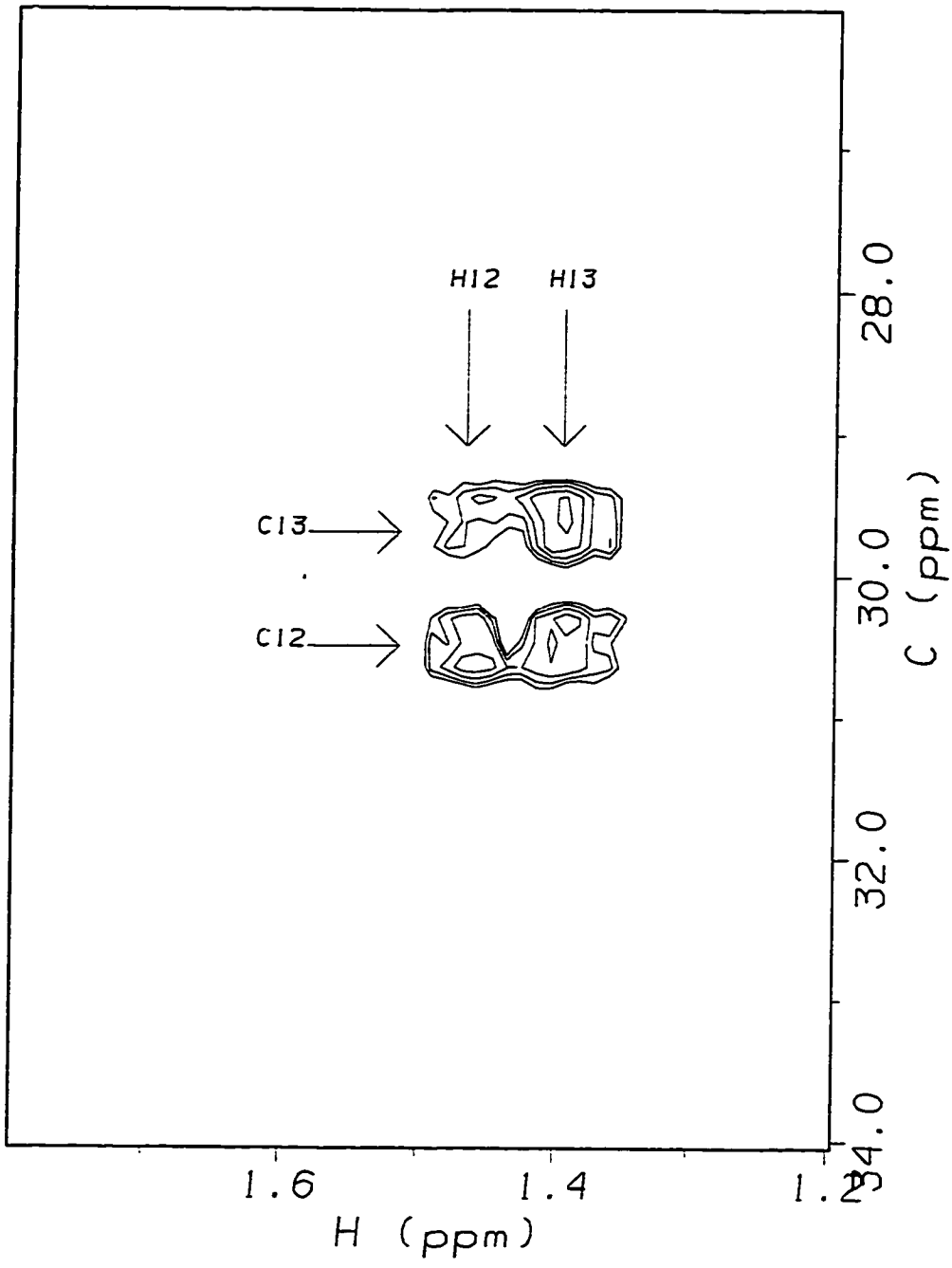

Figure 2.7: Two dimensional slice of the three-dimensional spectrum of molecule **Ib** in SDS which shows the crosspeaks between positions 12 and 13. 128 t1 (single quantum) and 120 t2 (double-quantum) points were acquired at 11.7T in 11 hours. The t1 and t2 sweep widths were 2750 and 2300 hz centered at 26.2 ppm.

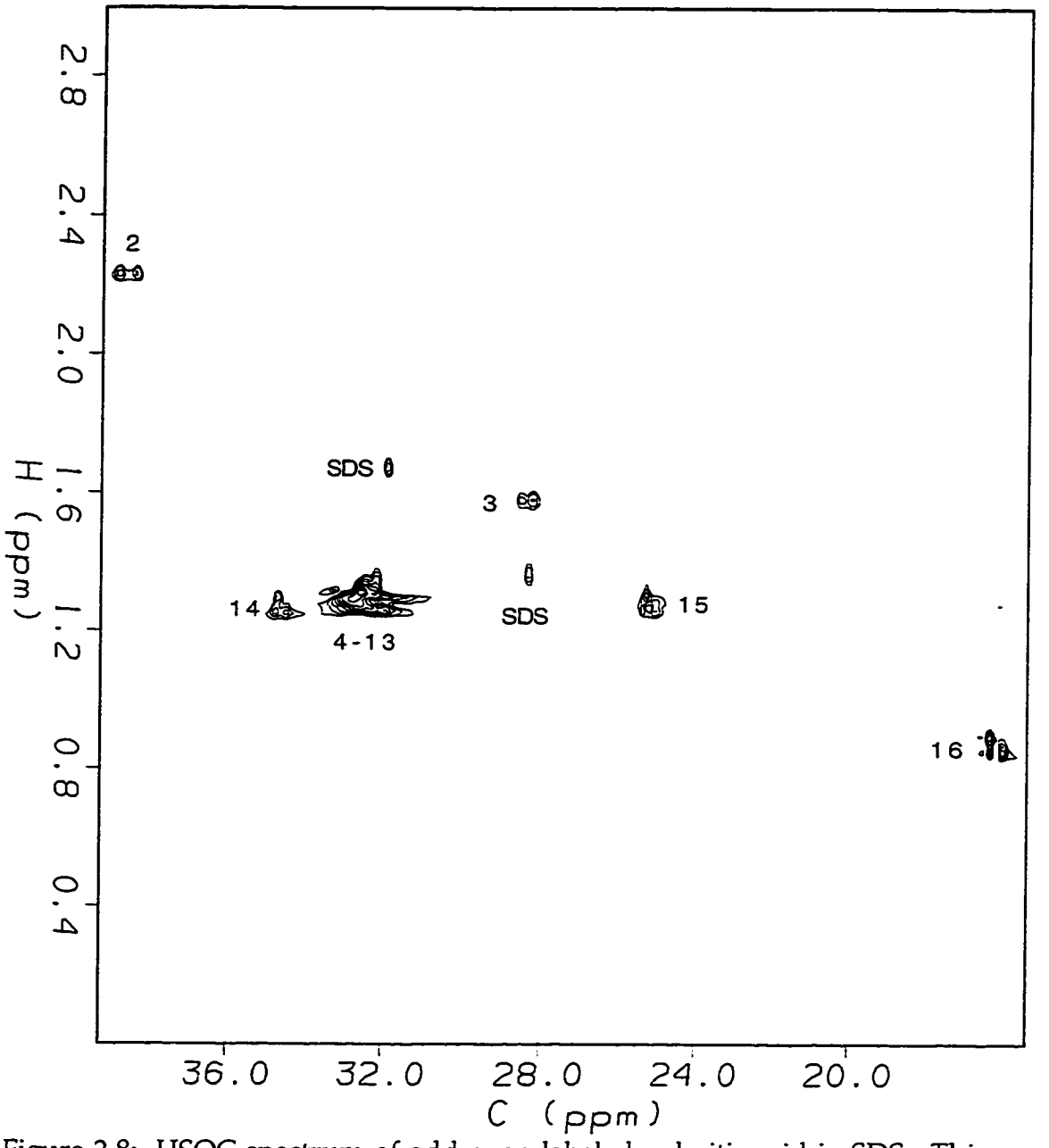

Figure 2.8: HSQC spectrum of odd-even labeled palmitic acid in SDS. This spectrum was acquired in 100 minutes on a Bruker AM500 spectrometer with 512 indirect FID's at 50°C.

Table II-A
Chemical Shifts for MHA in SDS[1]

Position	^{1}H ppm	^{13}C SQ ppm	^{13}C DQ ppm	^{13}C DQ calc
2	2.38	35.2	-8.4 (2,3 pair)	-8.3
3	1.71	25.5	-1.8	-1.8
4	1.42	30.1	8.0	7.9
5	1.42	30.2	3.1	3.3
6	1.42	30.3	8.8	8.8
7	1.49	30.9	2.6	2.7
8	1.19, 1.50	29.2	-7.2	-7.5
9	0.78	15.7	-25.6 f	-26.0
10	0.78	15.7	-7.3	-7.6
11	1.17, 1.49	29.1	2.2	2.3
12	1.46	30.6	7.8	7.9
13	1.37	29.7	4.5 f	4.4
14	1.34	32.1	2.7	2.5
15	1.34	22.7	3.4 f	-20.9
16	0.90	13.8		

[1]f indicates folded peak

Table II-B
Chemical Shifts for Palmitic Acid in SDS[2]

Position	^{1}H ppm	^{13}C SQ ppm	^{13}C DQ ppm	^{13}C DQ calc
2	2.23	38.6	4.0	4.0
3	1.58	28.4	-2.1	-2.1
4	1.32	32.5	2.3	2.4
5	1.32	32.9	2.4	2.4
6	1.32	32.5	2.7	2.6
7	1.30	33.1	2.9	2.9
8	1.30	32.8	3.0	2.8
9	1.29	33.0	2.7	2.6
10	1.28	32.6	3.0	2.2
11	1.28	32.6	2.3	2.8
12	1.28	33.2	1.9	2.3
13	1.26	32.1	3.8	3.7
14	1.25	34.6	-3.0	-3.2
15	1.27	25.2	-1.5 f (-21.5 u)	-21.5
16	0.85	16.3		

[2]f indicates folded peak, u indicates unfolded shift in ppm.

Chapter 3: MHA-ALBP Interactions

3.1 Introduction

The cytosolic fatty acid binding proteins (FABP's), a family of proteins which bind hydrophobic ligands, have been biochemically and structurally characterized over the past ten years (Glatz, et al., 1993). These proteins have the ability to bind a diverse group of lipids including long chain fatty acids and retinoids. The mode of binding is suggested by a series of x-ray crystallographic structural studies which show that the ligands are bound in a cavity formed between two beta-sheets (Banaszak, et al. 1994). The cavity is much larger in volume than that required for long-chain fatty acids and appears to contain a number of water molecules. Surprisingly, the positions and conformation of several long chain fatty acids are well determined in these structures. However, it is not clear at this point whether the conformation preferences exhibited in the solid state are carried over into solution and whether similar preferences are exhibited for other hydrophobic molecules. An investigation of these issues would be facilitated by methods applicable in solution and focused specifically on ligand properties as opposed to total structure determination.

Nuclear magnetic resonance (NMR) spectroscopy is a useful tool for gathering information about proteins and their ligands in solution. This has traditionally been accomplished using proton-proton NOE's and scalar

couplings (J-coupling). The usual approach is limited in the case of FABP's by several factors. FABP's are moderately large on the NMR scale, resulting in severely limited resolution for proton spectroscopy. With molecules such as long chain fatty acids where chemical shift degeneracy is great, resolution is even further compromised. These problems can be partially surmounted through the use of isotopically labeled ligands. Carbon-13 editing provides increased resolution and an ability to focus on the labeled ligand as opposed to the total protein-ligand complex (Rance, et al, 1987). For these reasons, carbon edited spectra were used in a recent study to selectively observe a retinoic acid ligand bound to a cellular retinoic acid binding protein, which is closely related to FABP's (Norris, et al., 1995).

As we will show here, the advantages of labeling can be extended for the highly degenerate resonances of an acyl chain by pairwise labeling and use of spectroscopic selection of double-quantum coherences (Norwood, 1992). In a double-quantum coherence, two coupled nuclei are excited together and resonate at the sum of their chemical shifts. This improves resolution by coupling nearly degenerate central carbons to better resolved positions nearer to the chain termini. Selection of two quantum coherences also suppresses natural abundance signals from underlying protein resonances by an extra factor of nearly 100, since it is rare to have two adjacent ^{13}C nuclei in a natural abundance protein sample. This is advantageous when working with large proteins where natural abundance background signal due to ^{13}C nuclei can be

quite significant. In addition, the use of carbon double-quantum spectroscopy leads directly to chemical shift assignments for the bound ligand by providing a pairwise correlation of all carbons. Definite chemical shift assignments may, in turn, be combined with J-coupling or NOE experiments to obtain structural constraints, or they may be interpreted directly in terms of preferred bound conformations. Structural analysis based on ^{13}C chemical shift perturbation proves of primary benefit in the system used here where NOE's and scalar couplings are difficult to obtain.

For this study, rat adipocyte lipid binding protein (ALBP) has been chosen as a prototype of FABP's because of a substantial body of previous biophysical characterization (Matarese & Bernlohr, 1988). It is readily available in amounts sufficient for NMR spectroscopy (Xu, et al., 1991), and its binding properties with a variety of ligands have been reported (Richieri, et al., 1994). Additionally, the structure of ALBP has been determined to high precision by x-ray crystallography in the presence of several different bound ligands (LaLonde, et al., 1994; Xu, et al., 1993).

Hydrophobic ligands were chosen from those which could readily be isotopically enriched by biosynthetic methods. In this initial study we have labeled and used cis-9,10-methylene-hexadecanoic acid. This is a naturally occurring fatty acid from *E. coli* (Cronan, J.E. Jr., et al., 1974) which is readily produced in useful quantities as the ^{13}C labeled species. MHA is similar in structure to oleic and palmitic acids, both natural ligands of ALBP. This

similarity to natural ligands allows comparisons to be made between solution data and crystal data.

3.2 Materials and Methods

Carbon-13 enriched sodium acetate was purchased from Cambridge Isotope Laboratories (Andover, MA) as 99% $^{13}C_{1,2}$ sodium acetate and as 99% $^{13}C_1$ sodium acetate. Sodium acetate in the 99% $^{13}C_2$ form was purchased from Isotec (Miamisburg, OH). Lipophilic sephadex type VI (lipidex) was purchased from Sigma (St. Louis, MO). *E. coli* strain LCD25 was supplied by Dr. J.E. Cronan, Jr. (U. Of Illinois) and *E. coli* strain JM101 containing the plasmid expressing ALBP was provided by Dr. L. Banaszak (U. of Minnesota).

Carbon-13 labeled fatty acids were produced biosynthetically using *E. coli* LCD25 as described in a previous chapter. ALBP was isolated from *E. coli* JM101 as previously described (Xu, et al., 1991). Briefly, *E. coli* were grown overnight supplemented M9 minimal media(Xu, et al., 1991). Ten ml of the turbid broth was added to one liter of fresh supplemented M9 media and incubated at 37° until the optical density at 550nm reached 0.5. Protein expression was induced by the addition of 50mg of nalidixic acid, and the culture was incubated for four hours. Bacteria were pelleted by centrifugation and dispersed in buffer. To release protein, cells were sonicated, centrifuged, precipitated with protamine, centrifuged, and stirred overnight in acetate

buffer at pH 5. After centrifugation of cell debris, soluble proteins were fractionated on sephadex G-75 resin. Fractions containing ALBP were identified by SDS-polyacrylamide gel electrophoresis (PAGE) and pooled. These fractions were passed over an imino-diacetic acid-sepharose column pretreated with copper sulfate. Histidine containing proteins, which comprised all major contaminants of crude ALBP, adhered to the column. Pure ALBP was collected in the flow-through. Purity at this point was judged sufficient by SDS-PAGE with Coomassie staining for use in NMR (about 95%). The identity of ALBP was confirmed by electrospray mass spectrometry.

Purified ALBP was delipidated using a lipidex column at 37° C and then incubated with a 5-fold excess of fatty acid at 37° C for 45 minutes. Unbound fatty acid was then removed by passage through lipidex at 4° C. ALBP samples were concentrated to 200µl after complexation with fatty acid using centricon-10 microconcentrators and placed in Shigemi NMR microtubes. All NMR experiments were performed at a concentration of 2-4 mM in protein.

NMR spectroscopy was carried out on a GE Omega 500 spectrometer equipped with a G17 pulsed field gradient accessory capable of generating gradients of 20 G/cm along 3 independent axes. Proton shifts were referenced to water at 4.75 ppm directly. Carbon shifts were referenced indirectly to water by using a frequency ratio of 0.251450200. The shifts reported in this chapter can be converted to the DSS standard by adding 2.5 ppm to carbon shifts and

subtracting 0.16 ppm from proton shifts (Wishart, et al., 1995).

Three-dimensional experiments were conducted using a modification of the proton-carbon single quantum-carbon double-quantum pulse sequence of Chung, et.al. (1993) as described in Chapter 2. Two-dimensional carbon double-quantum-proton (HCDQ) experiments were run using the same sequence except that carbon single quantum magnetization was not allowed to evolve. Proton-carbon single quantum correlation spectra were acquired using the enhanced sensitivity experiment of Kay, et al. (1992).

3.3 Results

After all experiments were refined on the SDS samples, spectroscopy was conducted on the protein-bound fatty acids. As expected, the HSQC experiment performed on the ALBP-**Ia** complex and shown in Figure 3.1 did not provide sufficient resolution or background suppression to make complete chemical shift assignments. Assignments for resolved positions similar enough to those in SDS to be assigned by inspection are labelled.

Although the three-dimensional experiments used on the SDS samples will work in principle on this system, their utility was limited by poor sensitivity. The effective fatty acid concentrations in this system were limited by protein solubility to only 10-20% of the SDS reference samples. Therefore, a two-dimensional version of the three-dimensional experiment was run by eliminating the carbon single quantum evolution period. The

resulting spectrum is simply a two-dimensional projection of the entire three-dimensional matrix. The two-dimensional spectrum does not have the resolving power of the complete three-dimensional experiment, but it represents a reasonable compromise between sensitivity and resolution while suppressing peaks from natural abundance sites. The proton shifts of resonances in this spectrum appear at the same position as in the HSQC spectrum. The carbon double-quantum shift is determined by the sum of the shifts of adjacent ^{13}C nuclei. The shifts used in calculating this sum are referenced to the carrier position rather than to 0 ppm, so that they may be positive or negative in sign. Resonances from ^{13}C nuclei without a neighboring ^{13}C nuclei are suppressed by the coherence selection gradient and do not appear in the spectrum.

The proton-correlated carbon double-quantum spectra for MHA-ALBP complexes are shown in Figures 3.2 and 3.3 for odd-even and even-odd patterns, respectively. Peaks at six separate double-quantum frequencies corresponding to odd-even pairs can clearly be distinguished in Figure 3.3. The carbonyl-alpha carbon pair is weak and is folded multiple times in the indirect dimension. The intensity of this resonance is diminished by transfer from only the CH_2 pair at the alpha position as the carbonyl has no directly attached protons. The absence of the C9-C10 pair is explained by several factors. First, the INEPT transfer in the three-dimensional experiment was optimized for methylene rather than methine spin systems, resulting in poor

excitation. Also, the near degeneracy of the carbon shifts makes excitation of double-quantum coherence inefficient. Accepting these explanations for missing and reduced intensity peaks, all eight possible pairs are accounted for. Note that in most cases a single elongated peak is observed at a given double-quantum frequency instead of the well resolved pair as seen in the SDS spectra. This results from line broadening upon binding which causes the proton resonances to be broader than the proton chemical shift difference between the resonances. Proton lines in these samples were 20-25hz which corresponds to 0.05 ppm. It may be seen from the final assignments in Table III-A that the difference in proton frequencies is less than this linewidth in most cases.

Assignments and shifts for positions not resolved in the HSQC are made in a manner analogous to that used for the SDS samples. Starting near the carbonyl, position 3 is known to be at proton shift of 1.54 from the HSQC spectrum (Figure 3.1). In the double-quantum spectra, only one double-quantum pair could represent position 3 on the basis of this downfield proton shift. The only carbon which could produce a double-quantum pair with position 3 in **Ia** is at position 4. A simple calculation using the known carbon shift of position 3 and the assigned double-quantum shift for the 3-4 pair gives the carbon shift at position 4 as 28.7. The shifts of positions 8, 11, and 13 may be determined in the same way from the known shifts of the cyclopropane carbons (positions 9 & 10) and carbon 14. For example, in Figure

3.3, the resonances at a double-quantum shift of -8.7 clearly arise from 8-9 and 10-11 pairs. Thus, the nearly degenerate shifts of positions 8 and 11 are determined. The shifts at positions 5, 7, and 12 are determined from the shifts of positions 4, 8, and 13, while position 6 is determined from positions 5 and 7. With only proton shifts to correlate double-quantum pairs in protein samples, there may be some ambiguities. However, redundant shift information from the odd-even and even-odd molecules helps to resolve this problem. While single quantum shifts are the same in both **Ia** and **Ib**, the different pairing leads to different double-quantum shifts. All measured double-quantum shifts appear in Table III-A, and they are compared to predictions based on the single quantum shift assignments.

Once assignments have been made for MHA in protein and SDS, the chemical shifts can be compared. Chemical shift differences between protein-bound and micelle forms are shown in Table III-B. There are several points to note: the changes in proton shifts are small, except at position 2 where they reach 0.4 ppm. The shift differences in carbon are larger, reaching more than 2 ppm; and these changes are not localized to sites near the carbonyl end. Clearly, the sources of these changes in chemical shift are complex. But as we shall document in the following discussion, a major contribution must be alterations in acyl-chain conformation. An analysis in these terms can give insight into conformations allowed in the binding site of ALBP.

3.4 Discussion

Several studies have previously examined the binding of ligand by FABP's. These include NMR studies using ^{13}C-carbonyl labeled fatty acids (Cistola, et al., 1988, 1989). While these studies provided useful data about binding stoichiometries and affinities, information about the conformation of bound fatty acids has come only from x-ray crystallography. These solid-state structures provide rich detail concerning ligand conformations, but information about ligand conformation and environment in the solution state would be very useful. A careful analysis of chemical shift perturbation provides some of this information.

The chemical shift assignments for the fatty acid MHA bound to ALBP are listed in Table III-B. At a qualitative level, it is significant that the diastereotopic methylene protons on C2 are resolved in chemical shift upon binding to protein. This change must be produced by binding to a chiral site such as the binding pocket of a protein. This observation confirms that protein-bound fatty acid is the species observed in these experiments. It is possible that the actual shifts observed are averages due to a rapid exchange between free and bound fatty acids. However, the solubility of the free fatty acid is quite low, and excess that might have existed in micellar form was removed by delipidation on a column. Thus, shifts should pertain to the bound acid alone.

There is a significant change in chemical shift of the C2 carbon and its attached protons on comparing SDS to ALBP. The magnitude and sign of this change are similar to that associated with increasing ionization of the carbonyl groups in a protein environment (Schaller & Robertson, 1995). Studies of rat liver FABP found a significant reduction in bound fatty acid pKa when compared to DPPC vesicles (Cistola, et al., 1988). It is likely that reduction in the fatty acid pKa is even more pronounced when compared to SDS. This occurs because both the surface charge and low dielectric environment in SDS influence the pKa of the fatty acid, destabilizing the deprotonated form of the fatty acid within the micelle. It is likely that a only small percentage of fatty acid is ionized at pH 7.5 in SDS. Ionization, therefore, increases on binding to ALBP, resulting in an upfield shift of the alpha protons and a downfield shift of the alpha carbon of the fatty acid. Several basic residues, arginine-106 and arginine-126, seen in crystal structures of ALBP near the binding site probably stabilize the ionized fatty acid through ionic interactions (Xu, et al., 1993). The change in proton shift for position 3 may also be related to a change in ionization at the carbonyl.

The assignments given in Table III-B indicate that there are significant changes in chemical shift relative to SDS throughout regions of the fatty acid further removed from the carboxyl group. Interpretation of the origin of these changes in shift is complex and involves such variables as the effective

dielectric constant of the medium, remote group effects, and local chain conformation.

The magnitude of the changes at several positions is outside the limits expected for remote group effects. Moreover, the changes in shift are not similar in size or direction when proton and carbon shifts at the same methylene position are compared. This contradicts expectations for remote group effects, which should perturb proton and carbon shifts in the same direction and to a similar extent. There is a general trend for many shifts in the carbon spectrum to be more upfield when bound to the protein. Such a systematic shift could be produced by a change in the effective dielectric properties representing the inside of the protein as compared to SDS. These changes are quite difficult to quantify. However, we might expect the interior of an SDS micelle to model a protein fairly well, and thus represent a not dissimilar dielectric environment. The environment in an SDS micelle is primarily hydrocarbon, but there is substantial water penetration, just as there is in the protein. Moreover the change of shifts in going from chloroform, with a clearly different dielectric constant, to SDS is marginal for producing the observed effects.

We therefore fall back on a conformational effect to analyze shifts. There is a relatively large upfield change of approximately 6 ppm in carbon chemical shift in going from a trans to a gauche methylene bond in alkanes with very little corresponding shift in proton resonance (Cheney & Grant,

1967; Batchelor, et al., 1974). This change in shift occurs in those carbons at opposite ends of the dihedral angle separating them. A similar conformational chemical shift effect is observed with protein backbone conformation and may be used for structure prediction (see, for example, Spera & Bax, 1991; de Dios, et al., 1993; Wishart & Sykes, 1994). In SDS, we would expect the fatty acid spectrum to reflect a dynamic equilibrium with contributions from both trans and gauche rotamers. Specifically, the distribution is assumed to be 67% trans based on the theoretical work of Jorgenson, et al. (1984). The chemical shift in SDS would reflect this, occurring near the center of this 6 ppm range. Several exceptions would be expected near the chain termini and adjacent to the cyclopropane ring. The absence of the gauche$^+$/gauche$^-$ interactions at the termini allows the distribution to shift towards gauche, while steric interactions with the cyclopropane ring change the distribution towards trans at adjacent positions (Batchelor, et al., 1974). These expected distributions are depicted as the black bars in Figure 3.4.

The chemical shift changes seen upon binding of MHA to ALBP would be expected to reflect a redistribution of rotamers from the equilibrium found in the micelle. Using SDS shifts and the expected population distribution as a reference, it is possible to calculate the trans-gauche rotamer distribution at each position for the ALBP bound fatty acid. A change from 100% trans to 100% gauche will be assumed to contribute a 6 ppm upfield shift to each

carbon at the end of a four-carbon dihedral angle. For all central carbons there will be two dihedral contributions to chemical shift, while terminal carbons are involved in only one carbon-carbon dihedral angle. The carbons alpha to the cyclopropane ring are fixed in a syn rotamer and also contain only one variable dihedral contribution to chemical shift. Beginning at the methyl end or with the methylenes near the cyclopropane group where only one dihedral angle makes a contribution to chemical shift, it is possible to extract dihedral populations at every site. For example C11 moves downfield by 1.3 ppm on binding to ALBP. This would correspond to a decrease of 21% in trans bond distribution. Calculated rotamer distributions for all sites are listed in Table III-C and shown graphically in Figure 3.4 as the gray bars.

It can be seen that at several positions along the chain a significant shift away from the 1:2:1 gauche(+):trans:gauche(-) equilibrium of the SDS sample is predicted. The 2-3, 7-8, and 8-9 bonds are shifted to a more trans distribution, while the 10-11 and 14-15 bonds show little redistribution. The regions from 3-7 and 11-14 show an increase in gauche populations. This increase is especially marked in the 3-4, 4-5, and 5-6 bonds. These redistributions may result from steric interference of protein side chains with the free rotation of the acyl chain or from specific hydrophobic interactions which favor a particular conformation.

X-ray crystallography has revealed trans carbon-carbon dihedral angles at most positions in ALBP-bound palmitic acid (Xu, et al., 1993). There are

four bonds which are in the gauche position in the solid state. These include bonds between carbons 4-5, 5-6, 9-10, and 13-14. A similar acyl chain conformation has been observed for other protein-bound fatty acid crystals (LaLonde, et al., 1994). This may indicate a preference of the protein for specific fatty acid conformations. Comparison between dihedral angles measured in the crystal structure of ALBP-palmitate and the distributions calculated for ALBP-MHA shows some similarities. The cis cyclopropane bond at the 9-10 position is a structural correlate of the gauche 9-10 bond seen in the crystal. The gauche bond at 13-14 is matched by an increase in gauche character at positions 11-14. Some increased motion in solution as compared to the crystal forms may allow this gauche bond to be distributed across three positions rather than being fixed at one bond. Finally, the pair of gauche bonds seen in the crystal at positions 4-5 and 5-6 is paralleled by a marked increase in gauche distribution in the 3-7 region of bound MHA. Again, there may be some increased flexibility when the protein-fatty acid complex is in solution.

Thus, using a simple conformational interpretation of ^{13}C chemical shifts, we see a marked similarity between fatty acid chains bound to ALBP in solution and fatty acids bound to ALBP in the crystal form. Unfortunately the absence of a crystal structure specifically involving MHA introduces some uncertainty in the comparison. Nevertheless, we can make a strong argument for the maintenance of preferred binding geometries for ALBP in

solution, much along the lines observed in the crystal. The preference is interesting because the binding pocket is sufficiently large to accommodate a variety of conformers. Xu et al. have speculated that an organized internal water network might contribute to conformational preference for a ligand (1993). Similar bound conformations were also seen for retinoic acid in complex with cellular retinoic acid binding proteins when crystal and solution forms were compared (Norris, et al., 1995). That study when considered along with this one suggest that bound conformations seen in crystal structures of FABP's may generally be preserved in solution.

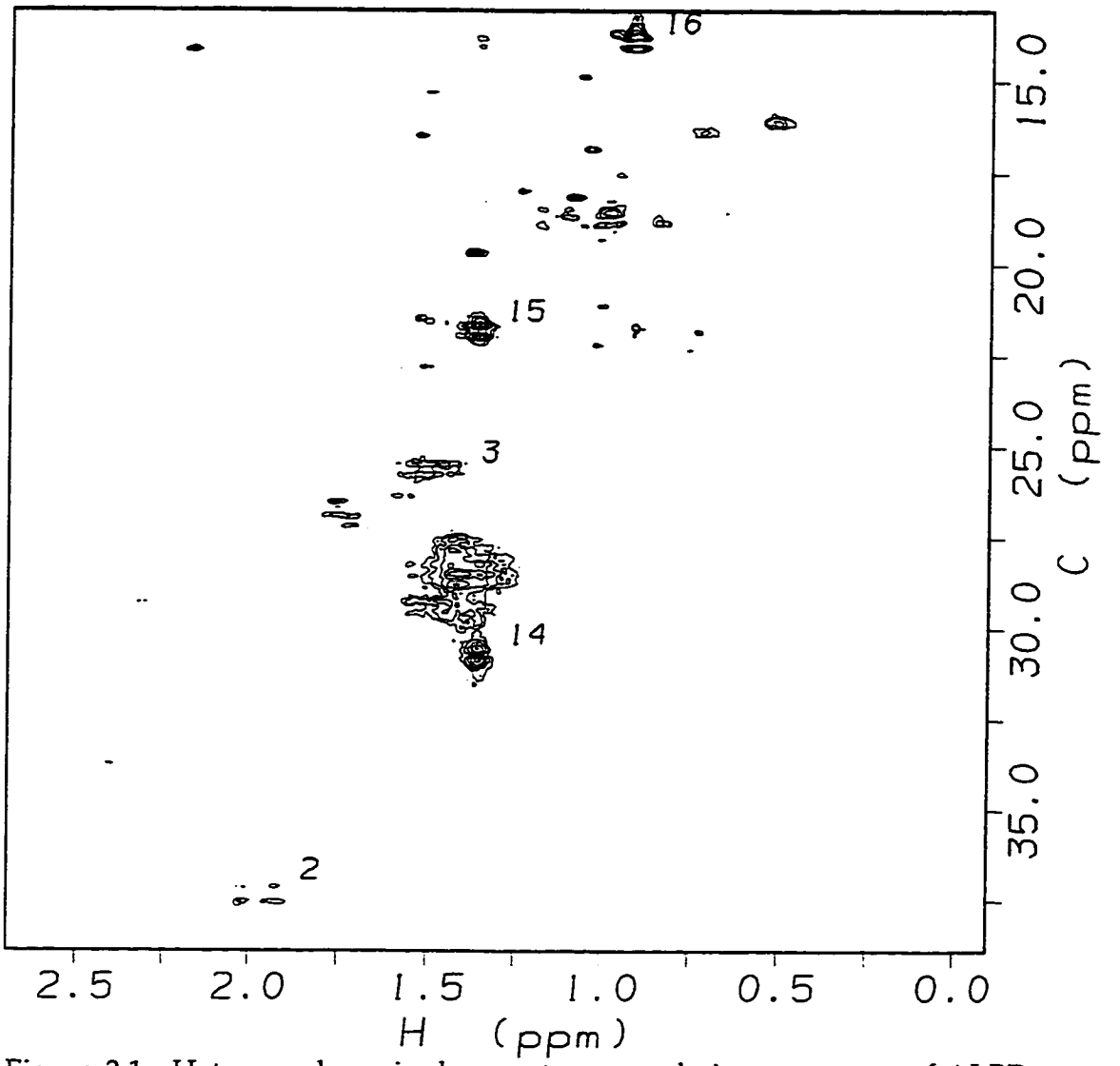

Figure 3.1: Heteronuclear single quantum correlation spectrum of ALBP-MHA complex at 37° C. A total of 440 t1 points were acquired with an indirect sweep width of 3750 hz. Data were acquired in 8 hours at 11.7T.

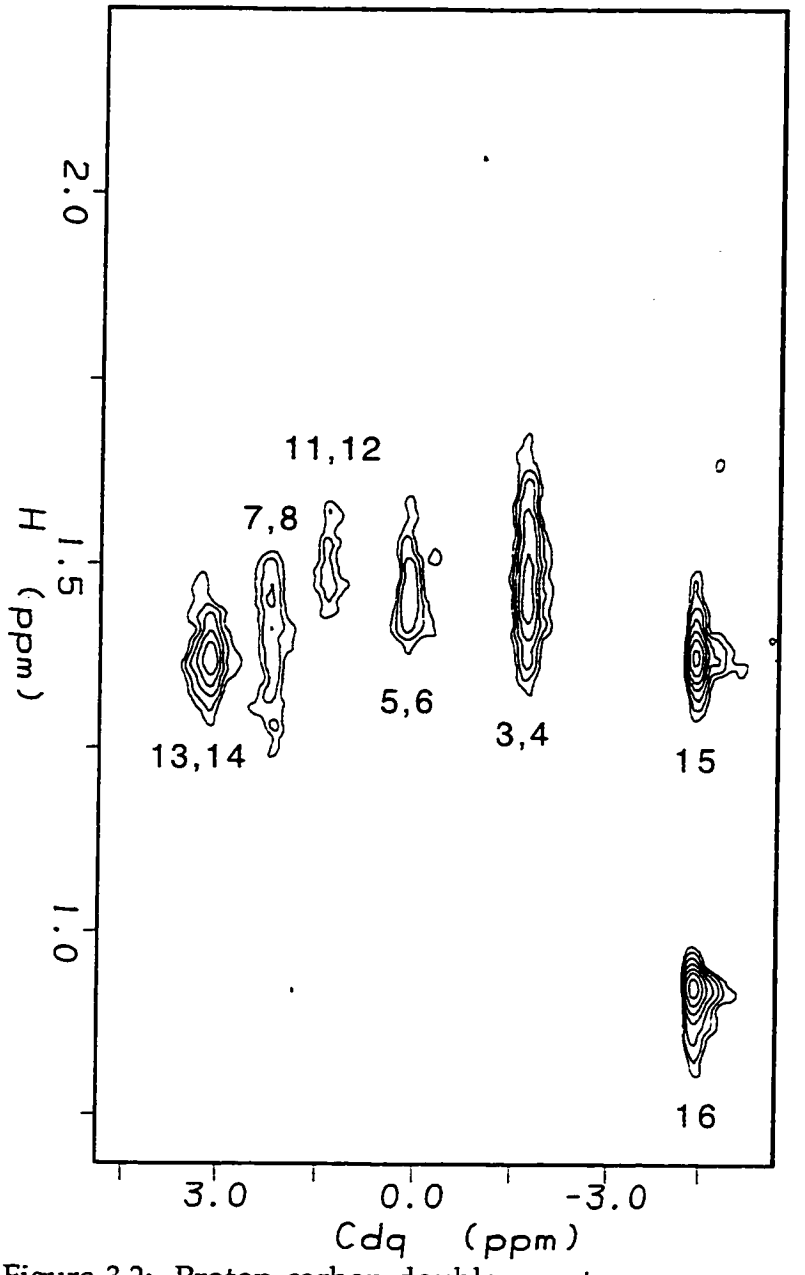

Figure 3.2: Proton-carbon double-quantum correlation spectrum of **Ia**-ALBP complex at 37° C. A total of 128 t1 points were acquired with an indirect sweep width of 2000 hz centered at 28.0 ppm. Data were acquired in 15 hours at 11.7T.

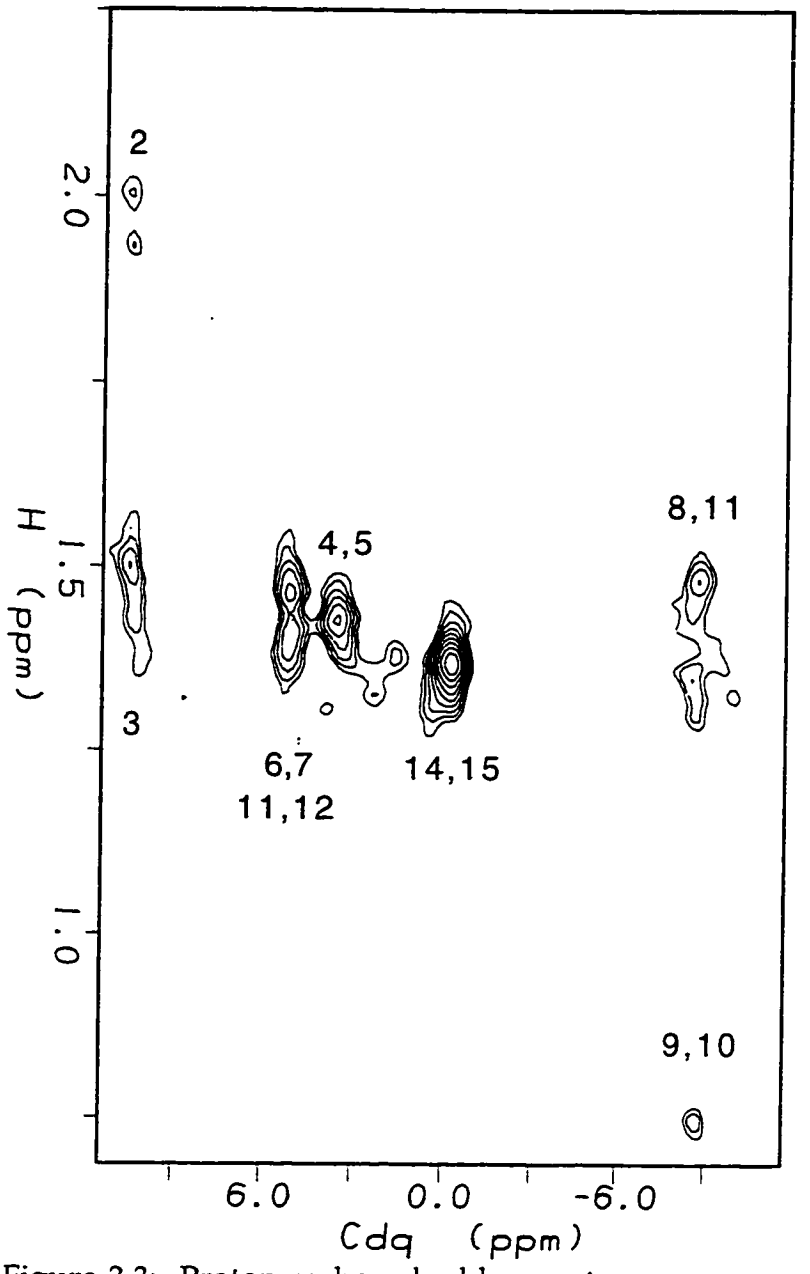

Figure 3.3: Proton-carbon double-quantum correlation spectrum of **Ib**-ALBP complex at 37° C. A total of 64 t1 points were acquired with an indirect sweep width of 2940 hz centered at 26.5 ppm. Data were acquired in 40 hours at 11.7T.

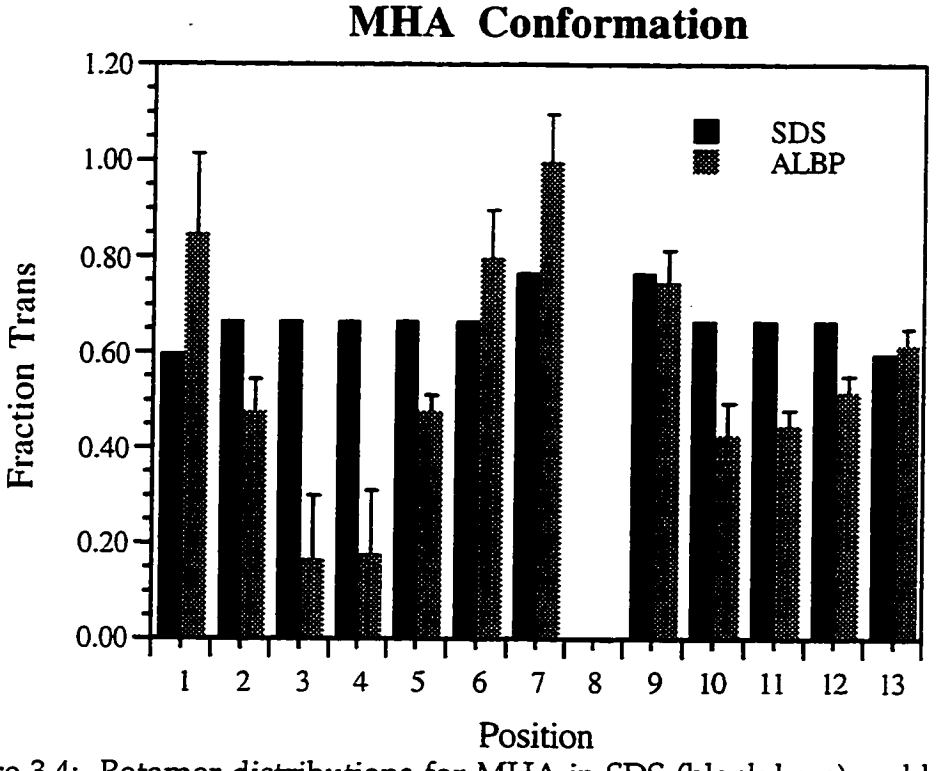

Figure 3.4: Rotamer distributions for MHA in SDS (black bars) and bound to ALBP (gray bars). Error bars are shown on the calculated values for the ALBP bound form and are based upon an uncertainty of 0.2 ppm in the measured carbon-13 chemical shift. Position 1 represents the dihedral angle involving carbons 1-2-3-4, and so on.

Table III-A
MHA Chemical Shifts in Complex with ALBP[a]

Position	Proton	Carbon SQ	Carbon DQ	Calc DQ
2	2.02,1.93	37.4	10.6 (2,3 pair)	10.0
3	1.54	25.6	-1.7	-1.7
4	1.44	28.7	3.7	3.7
5	1.43	28.0	0.1	0.1
6	1.47	28.1	5.1	5.2
7	1.46	30.1	2.2	2.2
8	1.25,1.50	28.1	-8.7	-8.6
9	0.75	16.4	Ø	-23.2
10	0.75	16.4	-8.7	-8.9
11	1.34.1.47	27.8	1.4	1.4
12	1.53	29.6	5.2	5.0
13	1.37	28.4	3.2	3.2
14	1.37	30.8	-0.2	-0.4
15	1.37	21.8	-20.4 f	-20.3
16	0.92	13.9		

[a]f indicates folded peak, Ø indicates peak not observed in spectrum. Shifts are given in ppm.

Table III-B
Changes in MHA Chemical Shift Between SDS and ALBP

		Proton Shift			Carbon Shift	
Position	SDS	ALBP	Change	SDS	ALBP	Change
2	2.38	2.02,1.93	-0.36,-0.44	35.2	37.4	+2.2
3	1.71	1.54	-0.17	25.5	25.6	+0.1
4	1.42	1.44	+0.02	30.1	28.7	-1.4
5	1.42	1.43	+0.01	30.2	28.0	-2.2
6	1.42	1.47	+0.05	30.3	28.1	-2.2
7	1.49	1.46	-0.03	30.9	30.1	-0.8
8	1.19, 1.50	1.25,1.50	+0.06,0	29.2	28.1	-1.1
9	0.78	0.75	-0.03	15.7	16.4	+0.7
10	0.78	0.75	-0.03	15.7	16.4	+0.7
11	1.17, 1.49	1.34.1.47	+0.17,-0.02	29.1	27.8	-1.3
12	1.46	1.53	+0.07	30.6	29.6	-1.0
13	1.37	1.37	0	29.7	28.4	-1.3
14	1.34	1.37	+0.03	32.1	30.8	-1.3
15	1.34	1.37	+0.03	22.7	21.8	-0.9
16	0.90	0.92	+0.02	13.8	13.9	+0.1

Table III-C
Conformationally Induced Chemical Shift Changes for MHA

Position	^{13}C Change	Conformational shift	Change in trans fraction
2	+2.2		
3	+0.1		
4	-1.4	1.5	+0.25±0.17
5	-2.2	-1.1	-0.19±0.067
6	-2.2	-3.0	-0.50±0.13
7	-0.8	-2.9	-0.49±0.13
8	-1.1	-1.1	-0.19±0.033
9	+0.7	+0.8	+0.13±0.10
10	+0.7	+2.1	+0.35±0.10
11	-1.3	0	0
12	-1.0	-0.1	-0.02±0.067
13	-1.3	-1.4	-0.24±0.067
14	-1.3	-1.3	-0.22±0.033
15	-0.9	-0.9	-0.15±0.033
16	+0.1	+0.1	+0.02±0.033

Chapter 4: Nuclear Magnetic Resonance Studies of Acyl Chain Conformation in Palmitoyl-Acyl Carrier Protein

4.1 Introduction

Soluble acyl carrier proteins (ACP's) as well as other homologous sequences found in multifunctional polypeptides play a central role in fatty acid synthesis (FAS) for all organisms. These proteins or their homologous domains serve as a cofactors in the individual steps leading to synthesis (Slabas & Fawcett, 1992). Soluble ACP additionally is a cofactor for a variety of reactions involving fatty acid modification and transfer (Guerra & Browse, 1990; Pugh & Kates, 1984).

Strucutral studies of the FAS systems are somewhat limited to date, with that of *Escherichia coli* being the best characterized. ACP from *E. coli* is a protein of 77 amino acids with a preponderance of acidic residues. The structure of ACP has been determined through the use of nuclear magnetic resonance (Figure 1.2), as has that of octanoyl-ACP (Holak, et al., 1988; Jones, 1991). In both the acylated and unacylated forms, ACP was found to fold into three roughly parallel alpha-helices connected by unstructured loops. The acyl chain in octanoyl ACP has been postulated to bind to a hydrophobic groove between the second and third helices which appears capable of accomodating a variety of acyl chains (Jones, et al., 1987a; Jones, 1991).

No detailed stuctural data have been collected on acyl carrier protein coupled acyl chains longer than eight carbons. The way in which these longer chains are accomodated and any accompanying changes in interactions

between the acyl chain and ACP may be important in enzymatic reactions such as the de-acylation event which terminates fatty acid synthesis (Spencer, et al., 1978). It is known, for example, that hydrolysis of thioesters by acyl-ACP hydrolase is selective for palmitoyl chains when the bond is to ACP as opposed to coenzyme A (Ohlrogge, et al., 1978).

NMR is a useful tool for studying ACP-acyl chain interactions as demonstrated by previous studies on octanoyl-ACP (Jones, et al., 1987b). It can be particularly useful with flexible proteins such as ACP (Kim & Prestegard, 1989) where dynamic as well as structural information can be acquired. Previous studies used fluorine labeling of the acyl chain in order to resolve the degenerate proton NMR spectra of long acyl chains (Jones, et al., 1987a; Jones, 1991). Fluorine-proton NOE contacts were measured to find acyl chain contacts with ACP. While this method was effective in overcoming the extreme chemical shift degeneracy found in acyl chains, it had several limitations as detailed in Chapter 1. To review, a different fluorinated acyl chain was synthesized for each location to be examined on the chain, making the study very labor intensive. It was not possible to synthesize 2- or 3-fluoro octanoyl-ACP, so these positions could not be studied. Finally, the chemical properties of fluorine are different from protons and could perturb the acyl chain-protein interactions. Thus, we seek in this study both to extend the range of acyl chains studied and to explore alternatives to fluorine-19 labeling for the resolution and characterization of acyl chain interactions.

Carbon-13 enrichment proves a viable alternative to fluorine-19 labeling. Through the use of single and double-quantum heteronuclear spectroscopy, good chemical shift resolution may be achieved. Most positions in palmitate (14 of 16) can be resolved and studied simultaneously, reducing

experimental time and thereby improving reproducibility and sensitivity. Those positions alpha and beta to the carbonyl which could not be studied with fluorine probes due to synthetic difficulties become readily accessible with ^{13}C labeling, and ^{13}C nuclei will also cause minimal perturbation of interactions. By filtering coherences through ^{13}C, proton NOESY data can be assigned and interpreted much like the fluorine-proton NOE data used in the octanoyl ACP study. Furthermore, as shown in the previous chapter, carbon chemical shifts can be interpreted in terms of acyl-chain conformation. These data may then be interpreted using the known solution structure of ACP (Holak, et al., 1988; Jones, 1991).

4.2 Materials and methods

Carbon-13 labeled fatty acids were produced biosynthetically using *E. coli* LCD25 as described in a previous chapter.

ACP was produced through an *E. coli* expression system as previously described (Hill, et al., 1995). The purification procedure was followed through the ion-exchange chromatography step described by Hill, et al. (1995). The product after this step is heterogeneous with 50% being devoid of the phosphopantotheine prosthetic group that normally carries the esterified fatty acid. At this point, holo-ACP was separated from apo-ACP by allowing the protein mixture to oxidize for 24 hours at 25° C in air. The dimerized holo-ACP ($[ACP]_2$) was then purified from the apo-ACP by using HPLC gel filtration on a Bio-Sil TSK-250 column. Purity of $[ACP]_2$ after one pass through the column was sufficient to eliminate the need for the reverse-phase HPLC step used by Hill, et al. (1995). The $[ACP]_2$ was reduced with

dithiothreitol immediately before use in the synthetase reaction described below.

Acyl-ACP synthetase was prepared through an *E. coli* expression system as previously described (Rock & Cronan, 1981; Jackowski, et al., 1994). The literature procedure was followed through the heat treatment step. The synthetase was then loaded onto a blue sepharose CL6-B column where it was used in an immobilized enzyme reaction without further purification (Anderson, et al., 1985).

Palmitoyl-ACP was prepared by catalyzing the addition of palmitic acid to ACP on the blue sepharose column. Forty mg (4.5 μmol) ACP and 1.3 mg (5.1 μmol) ^{13}C enriched palmitic acid were dissolved in 60ml of 0.1M TrisHCl pH 8.0/0.4M LiCl/10mM ATP/10mM $MgCl_2$/2mM DTT/0.07% Triton X-100. The mixture was recirculated on the column which contained bound acyl-ACP synthetase for 18 hours at 4° C. Palmitoyl-ACP was purified as described by Rock & Garwin (1979). The yield of this procedure was 40% based on ACP.

NMR samples of acyl-ACP were prepared at a concentration of 5mM in 50mM d_3-sodium acetate pH 6.0 (uncorrected)/D_2O. NMR experiments were conducted on a GE Omega 500 spectrometer equipped with a three-axis gradient accessory. Other experiments were done at 20° C. Proton chemical shifts were referenced to DSS as an internal standard at 0.00 ppm. Carbon chemical shifts were indirectly referenced to DSS as described by Wishart, et al. (1995).

Heteronuclear single quantum correlation experiments were done using the standard enhanced sensitivity experiment of Kay, et al. (1992). Three-dimensional proton-carbon-carbon correlation experiements were done as described by Chung et al. (1993) as described in Chapter 2 (Figure 2.4).

Two dimensional proton-carbon double-quantum (HCDQ) experiments were done with the same pulse sequence except that t_1 evolution was omitted.

The sequence for the two-dimensional HSQC-NOESY experiment is shown in Figure 4.4. This experiment was derived from a non-gradient selected HSQC (Bodenhausen & Ruben, 1980) as gradients resulted in an unacceptable reduction in signal intensity. Instead a 64 step phase cycle was used for coherence selection to reduce artifacts. This experiment was run with mixing times of 50, 100, and 200ms. The NOESY part of the experiment was run after the HSQC to take advantage of the increased chemical shift dispersion available after magnetization transfer had occurred to protein protons, since proton chemical shifts of palmitate are poorly dispersed.

4.3 Results

Several new aspects of the sample preparation were implemented in the course of this work and are worthy of comment. The expression system used for ACP produces significant amounts of apo-ACP (Hill, et al., 1995). Concern about competition of apo-ACP, which is inactive, for a site on the acyl-ACP synthetase column dictated that we should separate the apo- from holo-ACP before proceeding. Purification of holo-ACP by dimerization followed by a sizing column proved an effective replacement for the reverse phase HPLC used in the initial procedure. Dimerization occurs in air by disulfide formation between the sulfhydryls that terminate the prosthetic group on holo-ACP. *E. coli* ACP contains no cysteine residues so the prosthetic group contains the only sulfhydryl residues in the protein. Dimerization of ACP was complete by SDS-PAGE after 24 hours at pH 7.5 and 25° C. The dimer at twice the molecular weight is easily separated from

monomeric apo-ACP. A single gel filtration column effected near-baseline separation (see figure 4.1) and recovery of holo-ACP.

The acylation of ACP had been previously accomplished using chemical means. Chemical synthesis gives a poor yield and acylates multiple sites for palmitoyl-ACP (Cronan & Klages, 1981). The availability of an enzymatic reaction provides an effective way to produce large quantities of long-chain acyl-ACP's. An overexpression system for acyl-ACP synthetase was provided by Dr. Charles Rock, and this was an important prerequisite for this study. Our yield of acyl-ACP was 40-50% based on SDS-PAGE, which is somewhat lower that previously reported. This is likely due to the low ratio of fatty acid to ACP used. Due to the fact that ^{13}C labeled fatty acid was required, we were limited to using approximately equimolar amounts of fatty acid and ACP. Rock and Garwin (1979) were able to achieve nearly complete acylation by using a tenfold excess of fatty acid. Nonetheless, 40% yield is adequate for our NMR studies, and the ability to avoid multiple acylation sites is vital.

Chemical shift assignment of palmitic acid in SDS was described in chapter 2. The resolution was marginal for total assignment, even with the application of the three-dimensional double-quantum experiment. The acyl chain chemical shift resolution improves somewhat when palmitoyl-ACP is studied. The protein produces increased chemical shift dispersion in both the proton and carbon dimensions. Unfortunately, this is somewhat counterbalanced by the increased linewidth in the protein sample. The HSQC spectrum for odd-even labeled palmitoyl-ACP is shown in Figure 4.2. Resolved peaks are labeled in this plot, and their shifts are listed in Table IV-A. As with the SDS sample, a number of weak peaks arising from natural

abundance protein resonances are visible. Several changes from the SDS reference sample are evident. The diastereotopic proton pairs at positions 2, 4, and 14 are now resolved, with the shift difference between the proton pairs greatest at position 14. It is noteworthy that this can happen only in the asymmetric environment of the protein binding site. Proton shifts have changed to a more upfield position except for position 2. The carbon shift at position 2 is seen to be 7.8 ppm downfield from its position in SDS. To improve chemical shift resolution, carbon double-quantum spectroscopy was again used.

The three-dimensional experiment described for the SDS samples (Chung, et al., 1993) was used again with palmitoyl-ACP. As with the SDS data, two samples were produced using acyl chains with alternate labeling patterns. These experiments led to a straightforward assignment of the chemical shift for each position as described previously. The assigned proton and carbon shifts are listed in Table IV-A. In addition to the three-dimensional experiment, a two dimensional proton-carbon double-quantum experiment was used. This experiment was used to improve sensitivity; it also provides for simplified presentation of the data. The two-dimensional double-quantum spectra for the odd-even and even-odd samples are shown in Figures 4.3A and 4.3B, respectively. The double-quantum pairs are assigned and their shifts are tabulated in Table IV-B. Once again, double-quantum shifts were calculated from the assigned single quantum shifts and are shown in Table IV-B. These serve to confirm the listed assignments.

The acyl-chain chemical shift assignments of palmitoyl-ACP show differences from free palmitate in SDS throughout the chain. As noted in the HSQC spectrum, proton shifts are changed in an upfield direction throughout

the entire chain, with the average change being 0.28 ppm. The change is greatest at position 6, reaching nearly 0.5 ppm. Carbons at positions 4-7 are shifted in an upfield direction, with position 5 being shifted by 1.7 ppm. The carbons in the methyl portion of the chain are generally shifted downfield, although the change in shift is less that that seen closer to the carbonyl.

Introduction of a proton-proton cross-relaxation period after the ^{13}C chemical shift evolution provides a means of investigating through-space contacts. The acyl chain-protein contacts are of particular interest in this study. Cross relaxation for rigid systems depends upon the inverse of the sixth power of the interproton distance ($\frac{1}{r^6}$) and thus is visible only for close contacts. In mobile systems, some averaging occurs, but a qualitative interpretation is still possible.

The HSQC-NOESY experiment, shown in figure 4.4, was designed to maximize sensitivity and resolution in this system. Fatty acid proton shift was not allowed to evolve as the proton chemical shifts are essentially degenerate from positions 4 to 15. Thus no information would be gained from an indirect proton dimension, while the experimental time would be prolonged and sensitivity reduced. As designed, all magnetization eventually observed must have started on a ^{13}C attached proton. The magnetization is labeled with the ^{13}C frequency, then cross-relaxation to other protons occurs. Since the fatty acid is enriched in ^{13}C to a level of 30%, peaks originating on the fatty acid will dominate the spectra. However, highly degenerate resonances in the protein which also have efficient cross-relaxation can also appear. Cross-relaxation within the acyl chain is expected to dominate over weaker acyl-chain protein cross-relaxation. Crosspeaks to protein protons

give information about the chain's position in the three-dimensional structure of the protein.

We will begin by describing the HSQC-NOESY experiment with the 100ms mixing time, shown in figure 4.5. The 200ms mixing time is expected to exhibit more spin diffusion, while the 50ms mixing time suffers from poorer signal to noise. These experiments, therefore, will be used to confirm and expand upon the results of the 100ms mixing time experiment. Autopeaks from the fatty acid are the strongest peaks in this spectrum by an order of magnitude. Next in intensity are signals produced by cross-relaxation between protons within the acyl chain. These peaks can clearly be distinguished for positions 2 and 3, for example. A large number of autopeaks from natural abundance protein spin systems are also visible, since double-quantum filtering was not used to suppress them in this experiment. The can be found at many carbon frequencies which are not assigned to acyl chain resonances. Peaks which represent cross-relaxation between acyl chain protons and protein protons are found at the carbon frequency of the acyl chain proton-carbon pair and the proton frequency of the protein proton. These peaks are best resolved in the aromatic region of this spectrum. For example, crosspeaks are seen at the methyl carbon frequency and at proton frequencies of 6.45, 7.59, and 6.83 ppm. Since the spectrum was acquired in D_2O, amide protons undergo exchange and are not visible in this region. Therefore, these crosspeaks must belong to protein aromatic sidechain resonances.

Assignment of aromatic resonances in ACP is essential if these data are to be used in building a structural model. The aromatic region of the palmitoyl-ACP spectrum is quite similar to that of octanoyl-ACP (Mayo &

Prestegard, 1985), and the aromatic resonances may be assigned by comparison. The aromatic region of the proton spectrum is shown in figure 4.6 with assignments. The assignments in Figure 4.6 indicate that the crosspeaks at 6.45, 6.83, and 7.59 ppm arise from the aromatic resonances of tyrosine-71 and phenylalanine-50. No contacts are seen to phe-28 or to his-75 in the aromatic region of the spectrum. Another crosspeak to the methyl group is found in the less crowded upfield region of the spectrum at 0.04 in the proton dimension. The only corresponding shift in octanoyl-ACP is that of the isoleucine-72 gamma methyl at -0.05 ppm. Other crosspeaks to the methyl are seen at 2.41, 3.38, 3.42, and 3.79 ppm. These cannot be even speculatively assigned without performing a complete chemical shift assignment on palmitoyl-ACP.

The methylene at position 15 demonstrates aromatic contacts to tyrosine-71 but not to phenylalanine-50. Also seen is the peak at 3.79 ppm. No other crosspeaks are seen in the upfield region of the spectrum. The methylene at position 14 shows the same crosspeaks as those at position 15 in the 100 ms mixing time NOESY spectrum. Positions 5-13 are not resolved in this spectrum, so crosspeaks at a carbon frequency of approximately 32 ppm cannot be interpreted.

The crosspeak of position 4 with position 3 can be seen at 30.9 ppm, which is the carbon single quantum shift of position 4. A number of peaks are seen at this carbon frequency, including those with proton shifts of 2.40, 2.49, 2.62, 3.60, 3.88, and 4.02. The peaks at 2.40 and 2.49 ppm represent crosspeaks to position 2. Positions 2 (alpha) and 3 (beta) show few crosspeaks to the protein. The only peaks are at 3.84 and 3.98 ppm, which were also observed at position 4. These may represent contacts to the prosthetic group,

specifically to pantotheine gamma protons found at 4.02 ppm in octanoyl ACP.

The 50 ms mixing time experiment is essentially similar with weaker crosspeaks. The 200 ms experiment shows several additional crosspeaks which may be attributed to spin diffusion. For example, one of these additional peaks is seen between the palmitoyl methyl and a proton resonating at 0.48 ppm. Several possible assignments are suggested for the latter resonance, including isoleucine-62 delta methyl (0.42 ppm) and isoleucine-54 gamma methyl (0.44 ppm). However, this could also be the other gamma methyl of isoleucine-72 (0.56) shifted slightly upfield and appearing due to spin diffusion. While it is tempting to include data from the 200 ms set, these uncertainties suggest that it is best to use data from the shorter experiments for structural modeling.

4.4 Discussion

There are two principal sources of information about the nature of acyl chain-protein interactions that can be derived from the above presentation. These sources are chemical shift perturbations and NOE contact patterns. Differences in chemical shift are observed at a number of positions along the chain when an acyl-ACP is compared to the corresponding free acid in SDS micelles. Interpretation of these differences is complex because they are produced by a variety of factors. In this comparison, changes in chemical shift may arise from changes in chemical bonds, shielding by remote groups, and conformational changes in the acyl chain. These possibilities will be addressed in order.

The largest and possibly easiest change to explain is the downfield shift of the carbon and protons at position 2. These changes can be attributed to thioester bond formation between the palmitoyl chain and the prosthetic group. Comparison of butyric acid and S-methyl thiobutanoate as model compounds reveals proton and carbon shifts of 2.35 and 36 ppm for the butyric acid alpha position, with shifts of 2.55 and 46 ppm for the S-methyl thiobutanoate alpha position (Pouchert & Behnke, 1993). These shift differences closely parallel the data for palmitic acid and palmitoyl-ACP.

Remote group effects are harder to predict and quantitate. Side chains found in ACP which would be expected to produce particularly large remote group effects include phenylalanine and tyrosine. These effects are caused by ring currents and can exceed one ppm. ACP has two phenylalanines, one tyrosine, and one histidine. Based on the solution structure of ACP (Holak, et al., 1988) the two phenylalanines and the tyrosine lie in the proposed acyl chain binding site. If the chain were to lie along the face of the rings a substantial upfield shift would be expected. One useful characteristic is that remote groups should perturb shifts of protons and their directly attached carbons in the same direction and by about the same number of ppm. It is clear from the substantial difference in ^{13}C and proton shift perturbations that these cannot be the only source of perturbation. Thus, while they may explain the 0.15 to 0.40 change in proton shifts, remote group effects alone cannot account for the changes seen in ^{13}C shifts.

Carbon chemical shift can be influenced by conformational effects. As noted in a previous chapter, there is a 6 ppm upfield change in carbon chemical shift when going from a trans to a gauche dihedral angle in a linear alkyl chain (Cheney and Grant, 1967). This change is thought to be caused by

steric effects, as it occurs at the two carbons which move closer to one another when the dihedral angle changes. Attached protons as well as the two central carbons which define the dihedral angle are minimally affected. We will use this shift effect in an attempt to define the conformation of the acyl chain. A redistribution from all-trans to all-gauche should be reflected by a 6 ppm upfield change. Since the chain is in a state of constant conformational flux which is in the fast exchange limit on the NMR time scale, the changes will actually represent the redistribution in the fraction of time spent in the trans and gauche positions and will in all likelihood fall in the middle of this 6 ppm range.

To make the interpretation more straightforward we will attempt to eliminate the effect of remote groups by subtracting the proton chemical shift change at each position from the carbon shift change. The corrected shifts at positions 14-16 contain a contribution from only one dihedral angle and therefore can be used directly to determine the conformational change. For example, the shift of +1.0 ppm at position 16 represents an increase in trans distribution of (1.0/6.0) = 0.167. The shifts at positions 4-13 contain contributions from two dihedral angles. To determine the conformational shift for a single bond, these shifts must be corrected by subtracting the conformational shift for the other bond. If we start with the 16-13 pair this can be done by sequentially moving toward the thioester bond. For example, the corrected shift change of position 16 is subtracted from the corrected shift change for position 13. The residual difference, 0.7 ppm, is then used to determine the conformational change in the 11-12-13-14 dihedral angle. All shifts and calculations are tabulated in Table IV-C. This calculation was not performed at positions 2 and 3 as the shift at these positions is affected by the

the thioester bond as discussed previously. In addition, information at this position is redundant with that provided by positions 5 and 6.

The dihedral angle distribution for palmitic acid in SDS is expected to be approximately 0.6 trans and 0.4 gauche based on the theoretical work of Jorgenson, et al. (1984). In longer chains, there is an additional 0.07 trans fraction in the center of the chain due to unfavorable gauche$^+$/gauche$^-$ interactions (Batchelor, et al., 1974). This distribution is shown in Figure 4.7 along with the differences found based on the chemical shift analysis. The accuracy of the carbon shifts is approximately 0.2 ppm based on the digital resolution of the spectra. Calculations in Table IV-C were carried out to additional precision to avoid rounding errors. Error bars reflecting the accuracy of the chemical shift conformational analysis and the propogation of these errors are shown along with the data in Figure 4.7.

The conformational analysis indicates a significant change towards more gauche character at the dihedral angles defined by positions 1-2-3-4, 2-3-4-5, and 3-4-5-6. There is a possible shift towards trans character at the next three dihedral angles. However, the size of the change seen is on the order of the experimental error. There is a small change towards gauche bond character at the dihedral angles encompassing positions 8-9-10-11 and 9-10-11-12. Finally, the terminal three dihedral angles exhibit small but significant redistributions towards trans character. Overall, these data suggest that the acyl chain on average has bends around positions 3, 4, 5, and 10 with the remainder of the chain in a predominantly extended conformation.

HSQC-NOESY data can indicate regions where the acyl chain contacts the protein. The acyl chain is, of course, covalently attached to the protein through the prosthetic group at serine-36. Table IV-D summarizes the

observed non-covalent protein contacts. The identified contacts are well removed both sequentially and spacially from the covalent attachment site at serine-36.

There are few structural differences between ACP-SH and octanoyl-ACP (Jones, 1991). It is unlikely that there is a major structural rearrangement in going from octanoyl-ACP to palmitoyl-ACP. Therefore the structure of ACP-SH can be used as a basis for building models of palmitoyl-ACP to interpret the above contacts. Using the structure of ACP-SH as a model, we can see that the contacts found in the NOESY experiment between positions 14, 15, and 16 and the protein appear to occur in a similar spacial region of the protein. These contacts are with phenylalanine-50, tyrosine-71, and isoleucine-72. While tyrosine-71 and isoleucine-72 are distant from phenylalanine-50 in the primary sequence, they are neighbors in the three-dimensional structure of octanoyl-ACP. Specifically, their side chains lie in a hydrophobic pocket formed by the C-terminal ends of helices II and III. The data indicate that this pocket binds the methyl end of the palmitoyl group in solution. This finding is consistent with the hypothesis that the binding site for the acyl chain lies between helices II and III (Kim & Prestegard, 1989).

These data are complementary to previous work in this laboratory on octanoyl-ACP (Jones, 1991). That work used a shorter chain and examined different contact sites by replacement of specific protons on the chain with fluorine-19. It was not previously possible to gather data from the alpha and beta positions of the chain due to difficulties in synthesizing the appropriate fluorinated acyl chains. Data were collected for positions 4 through 7 of octanoyl-ACP and interpreted in terms of the solution structure of that complex. The chain appeared to be better constrained at its carbonyl end with

the methyl terminus making a variety of contacts with residues separated by significant distances in the three-dimensional structure (Jones, 1991). Most of the acyl chain-protein contacts were in helix II or in the loop between helices II and III (see figure 4.8).

One area of overlap between these studies is at position 4. Of interest is the fact that peaks are not seen for the contacts observed at position 4 in 4,4-difluoro-octanoyl ACP (Jones, 1991). These contacts were to protons of phenylalanine-28 (6.75, 6.90, 6.95 ppm), leucine-42 (0.59, 0.73) glutamate-60 (2.01, 2.31), or alanine-68 (1.62). There are several possible explanations for this observation. One is that the sensitivity of the experiment is inadequate to detect these contacts. This is unlikely since a number of alternate weak but unidentified contacts are seen for position 4. Secondly, the fluorine probe may have changed the interactions between the acyl chain and ACP. But this seems unlikely since the terminal end makes contacts in the same hydrophobic groove as seen in this study. Finally and most likely, the interaction between the acyl chain and the protein may change as the chain grows in length. Our data indicate that there are few contacts at the carbonyl end of the chain. Positions 2 and 3 show only two crosspeaks other than to each other, and it is possible that these are prosthetic group contacts. As detailed above, position 4 shows none of the crosspeaks seen in previous studies. Thus, this part of the acyl chain appears to lie in a position different from that which it occupies in octanoyl-ACP. Very likely the acyl chain is extended away from the protein surface.

We can now begin to build a model using the conformational data. To review, the ^{13}C shift derived structural data indicates that there are bends near the carbonyl end of the chain. The NOE data indicate that there are few

protein contacts near the carbonyl end of the acyl chain at positions 2, 3, and 4. Contrariwise, there are a number of contacts seen between the methyl terminus of the acyl chain and a hydrophobic pocket composed of phenylalanine-50, tyrosine-71, and isoleucine-72. Hydrophobic chromatography has suggested that the acyl chain binding site of ACP can accomodate six to eight carbons of a chain (Cronan, 1982). There is a monotonic increase in hydrophobic interaction strength for chain lengths from 10 to 18. However, chains of 8 carbons or fewer interact less strongly than expected, suggesting that they are tightly bound to ACP.

In octanoyl-ACP these data were interpreted to suggest that the acyl chain near the thioester bond was tightly bound and the methyl terminus was more mobile. An analagous model for palmitoyl-ACP does not satisfy the data presented here. One model which could satisfy these data involves extending the prosthetic group and proximal acyl chain near the thioester bond into solution. The chain bends back towards the protein in this model and positions 9-16 are bound in the hydrophobic pocket between helices II and III. A diagram illustrating this hypothetical model is shown in Figure 4.9.

A model such as this could have functional significance. The carbonyl end of the acyl chain is the site of elongation by the cellular synthetic machinery. The thioester bond is transiently broken and a two-carbon fragment from malonic acid is inserted. The thioester bond is also the site that must ultimately be cleaved when the chain reaches full length. Therefore, we can speculate that having the carbonyl end relatively mobile and exposed would facilitate the action of the FAS enzymes. These data indicate that the terminal eight carbons of the palmitoyl chain are those which interact with the binding pocket, while those carbons closer to the

prosthetic group and the prosthetic group itself are likely mobile and interact with solvent molecules. Once the growing chain reaches the appropriate length, it may adopt a unique conformation on ACP, facilitating recognition by the deacylase.

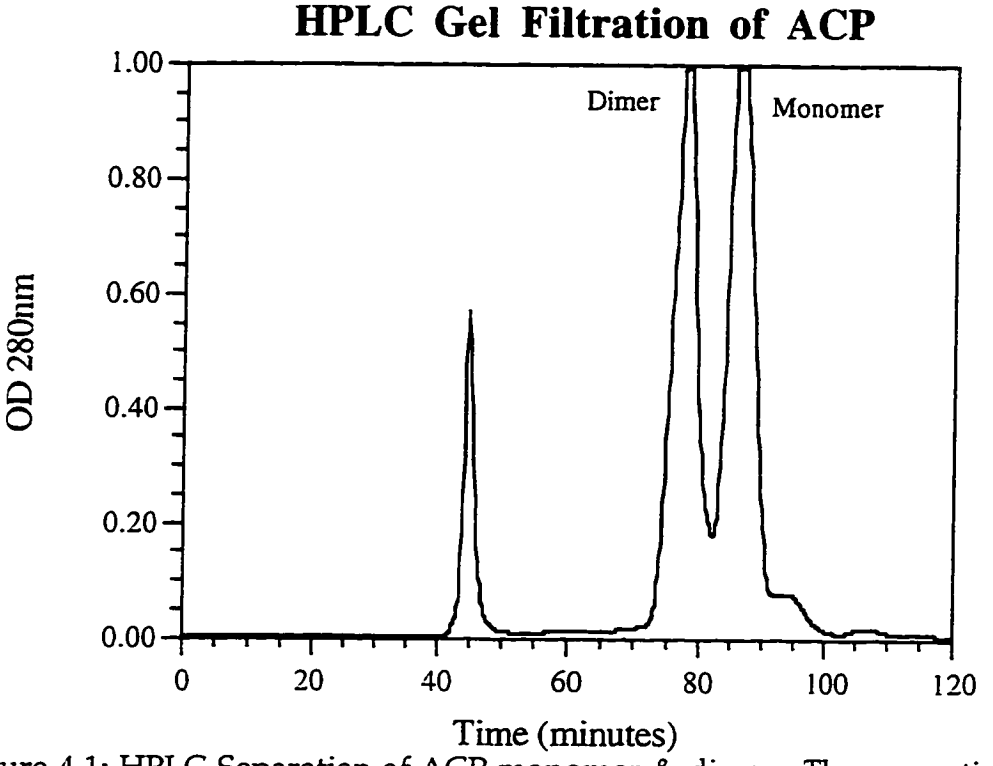

Figure 4.1: HPLC Separation of ACP monomer & dimer. The separation was done on a gel filtration column.

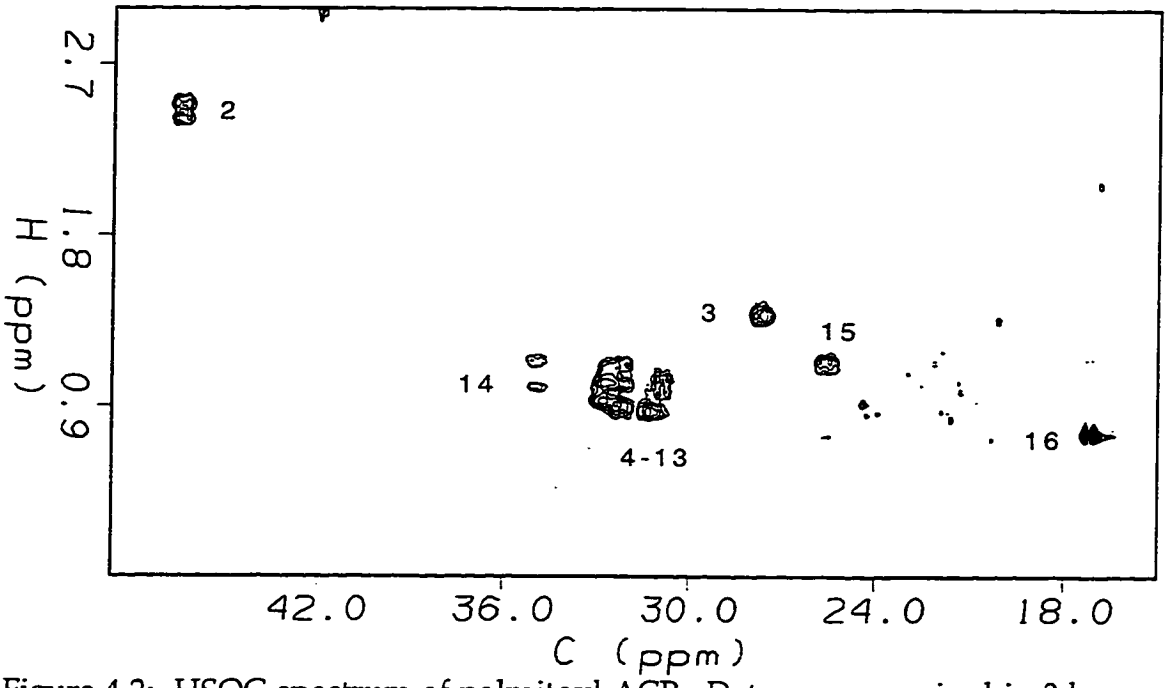

Figure 4.2: HSQC spectrum of palmitoyl-ACP. Data were acquired in 3 hours on a GE Omega 500 spectrometer with 512 indirect FID's at 20° C.

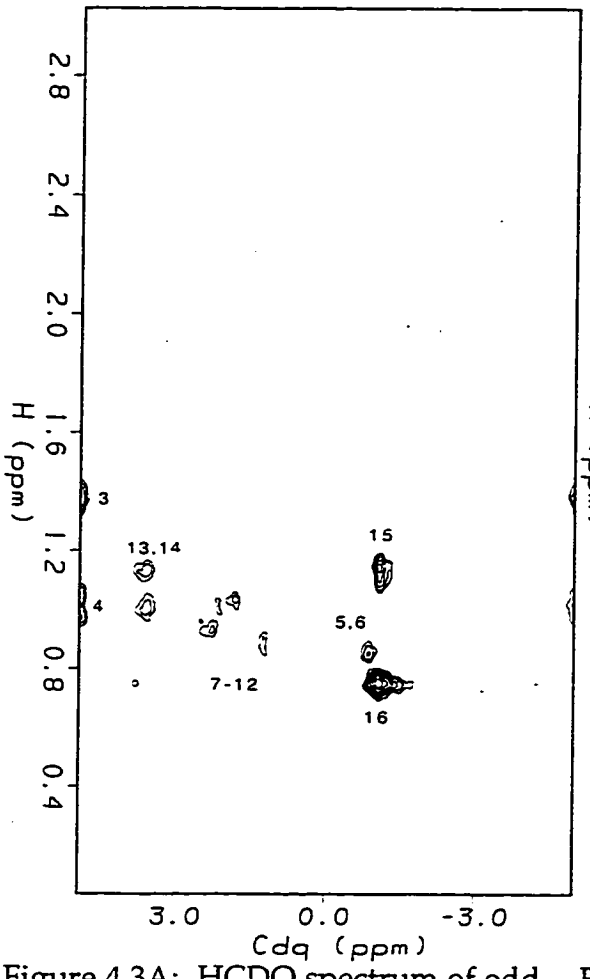

Figure 4.3A: HCDQ spectrum of odd-even labeled palmitoyl-ACP. Data were acquired in 11 hours on a GE Omega 500 spectrometer with 128 indirect FID's at 20° C

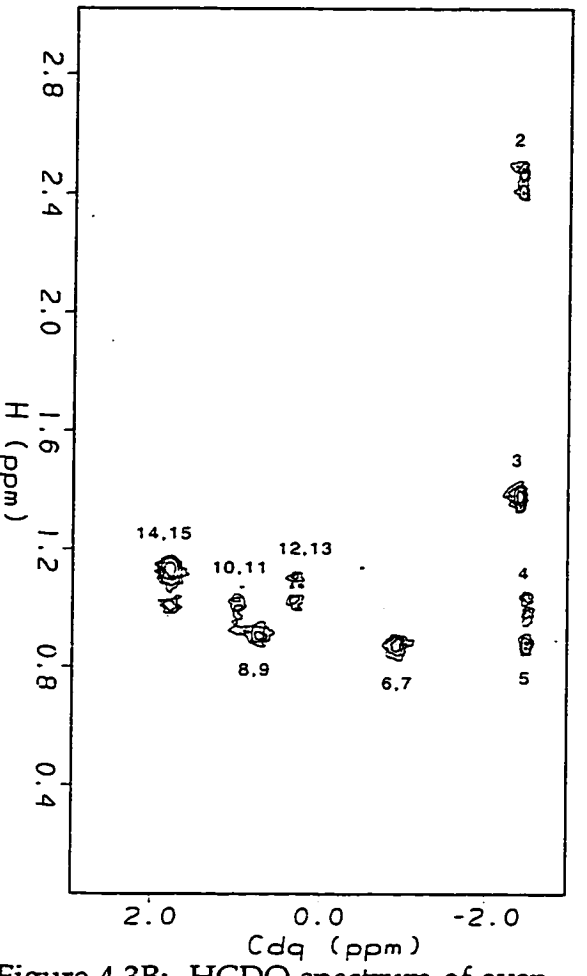

Figure 4.3B: HCDQ spectrum of even-odd labeled palmitoyl-ACP. Data were acquired in 11 hours on a GE Omega 500 spectrometer with 128 indirect FID's at 20° C

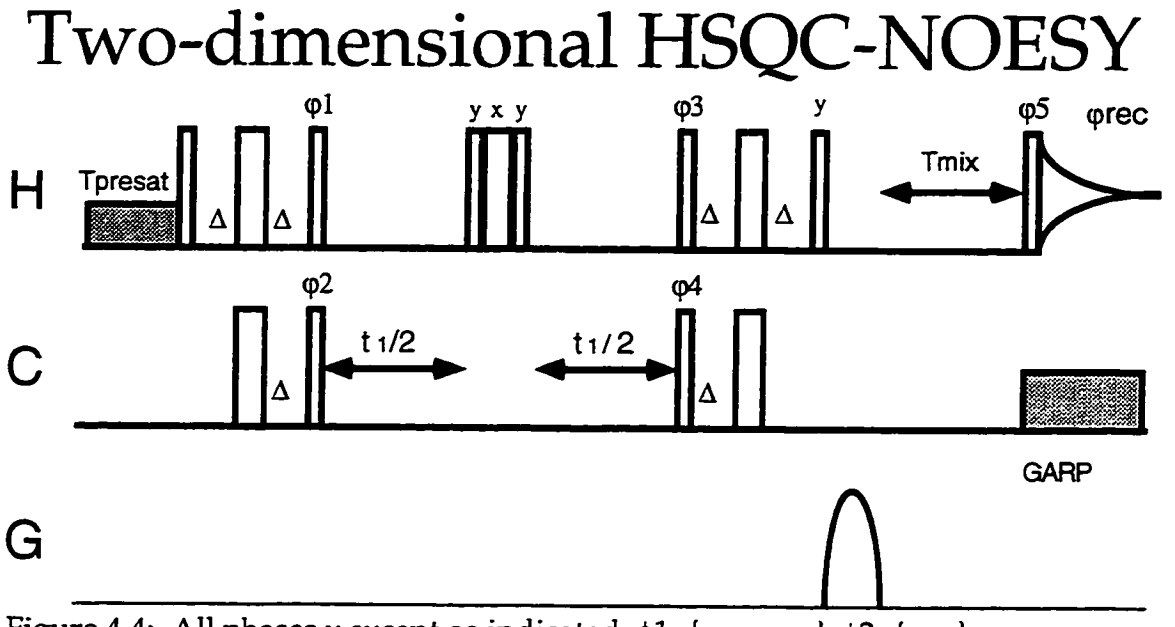

Figure 4.4: All phases x except as indicated: ϕ1={y,y,-y,-y}; ϕ2={x,-x}; ϕ3={4(x),4(-x)}; ϕ4={8(x),8(-x)}; f5={16(x),16(y),16(-x),16(-y)}; ϕrec=ϕ1+ϕ2 +ϕ3+ϕ4+ϕ5; Δ=1/(8JCH). JCH was 125 Hz. Quadrature detection in t1 was hypercomplex (states-tppi).

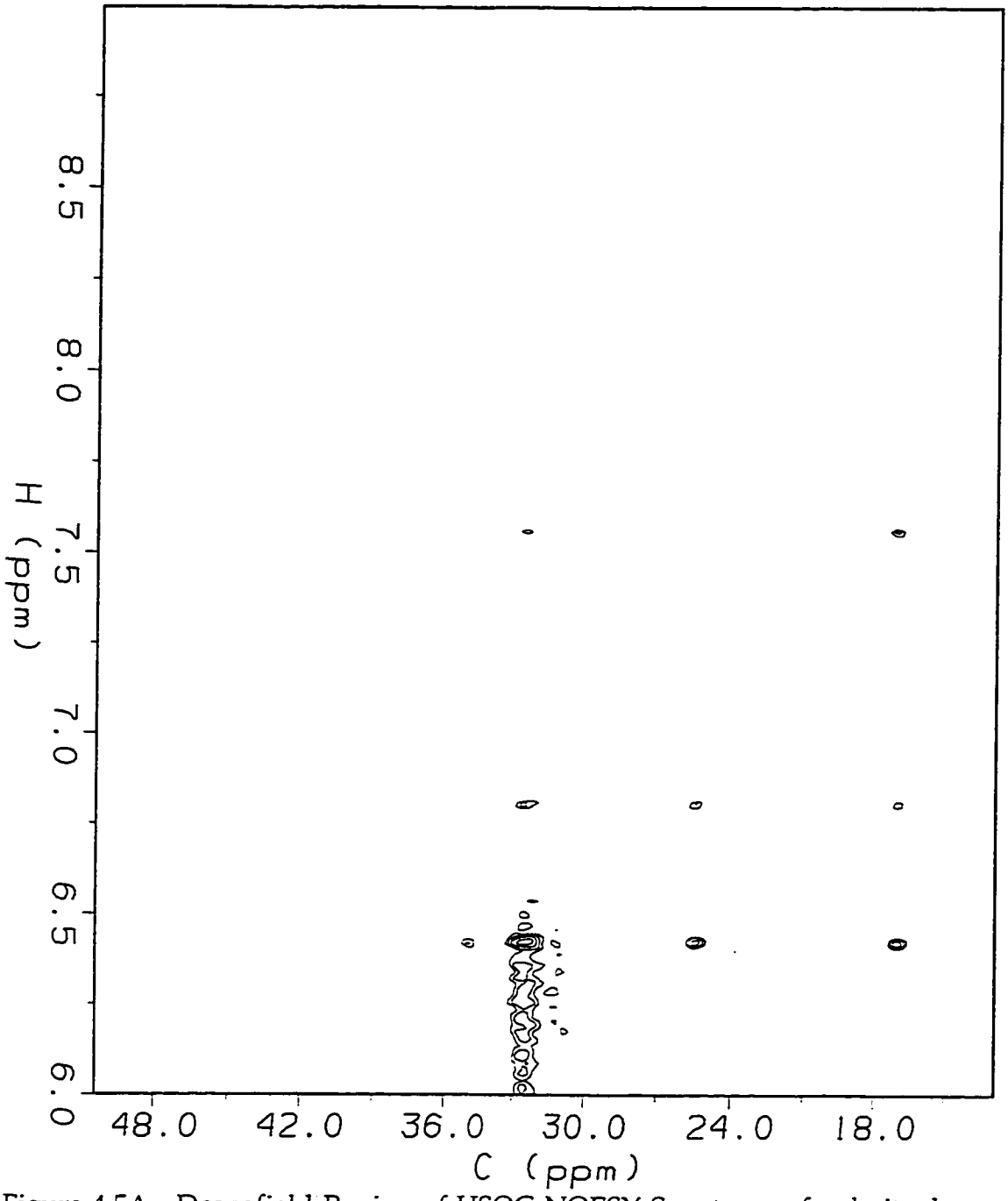

Figure 4.5A: Downfield Region of HSQC-NOESY Spectrum of palmitoyl-ACP. This spectrum was acquired with a 100ms mixing time using the pulse sequence of Figure 4.4. Data were acquired in 18 hours at 11.7 T and 37° C with 256 indirect FID's.

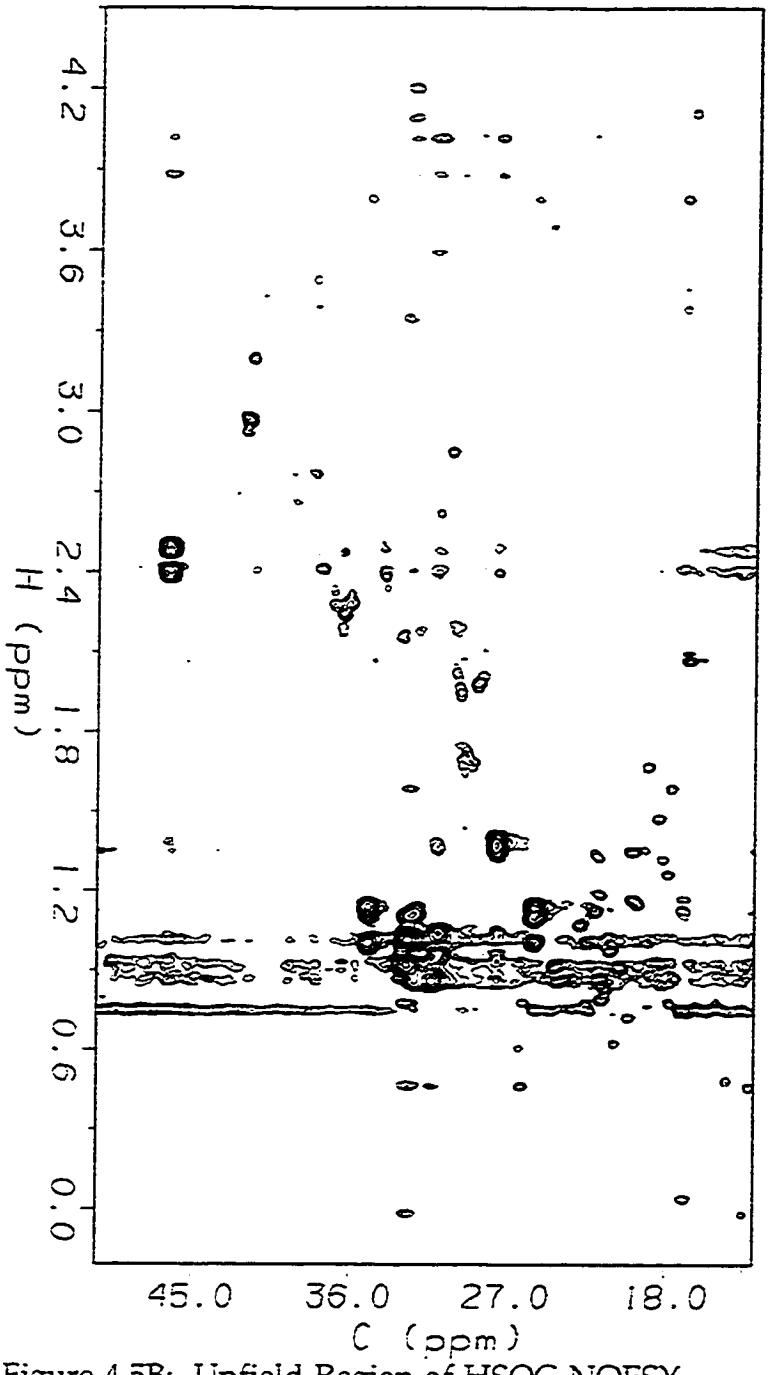

Figure 4.5B: Upfield Region of HSQC-NOESY Spectrum of palmitoyl-ACP. This spectrum was acquired with a 100ms mixing time using the pulse sequence of Figure 4.4. Data were acquired in 18 hours at 11.7 T and 37° C with 256 indirect FID's.

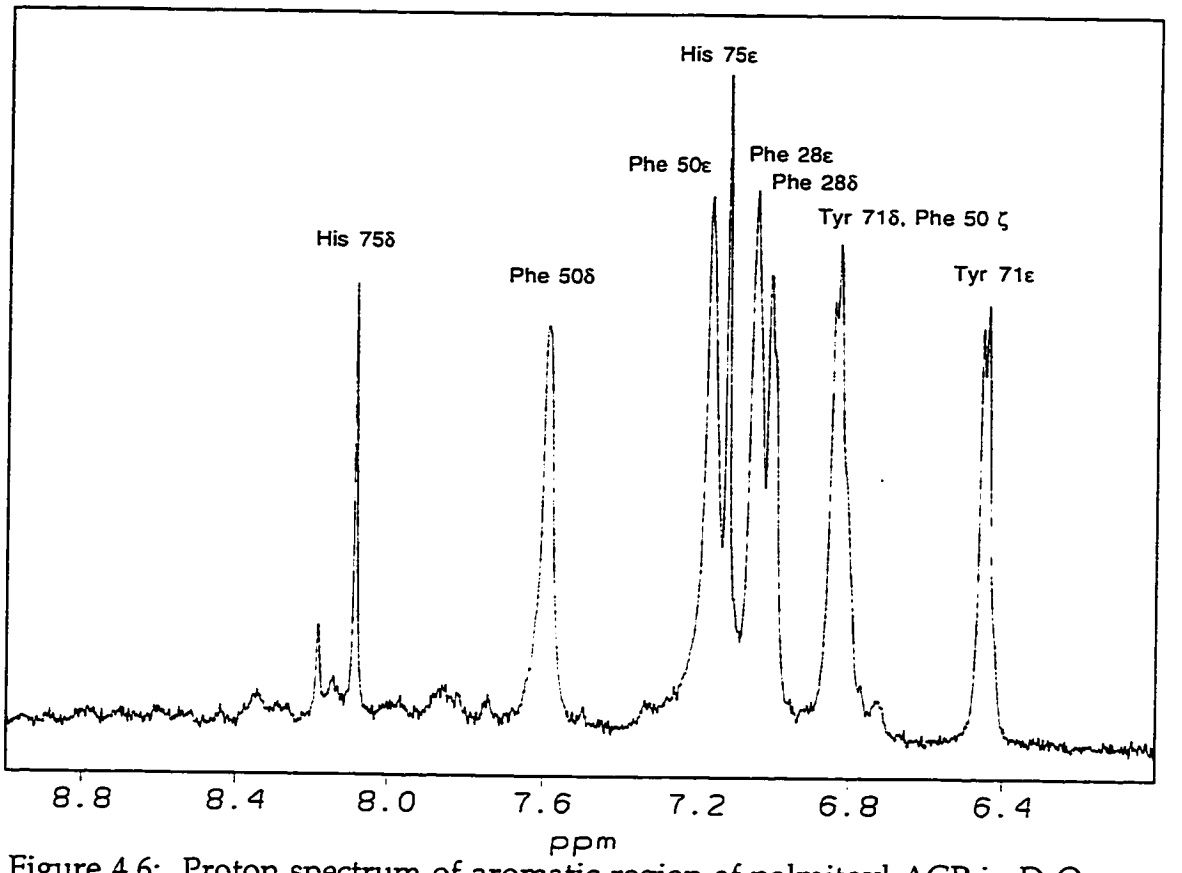

Figure 4.6: Proton spectrum of aromatic region of palmitoyl-ACP in D_2O. Assignments are transferred from octanoyl-ACP.

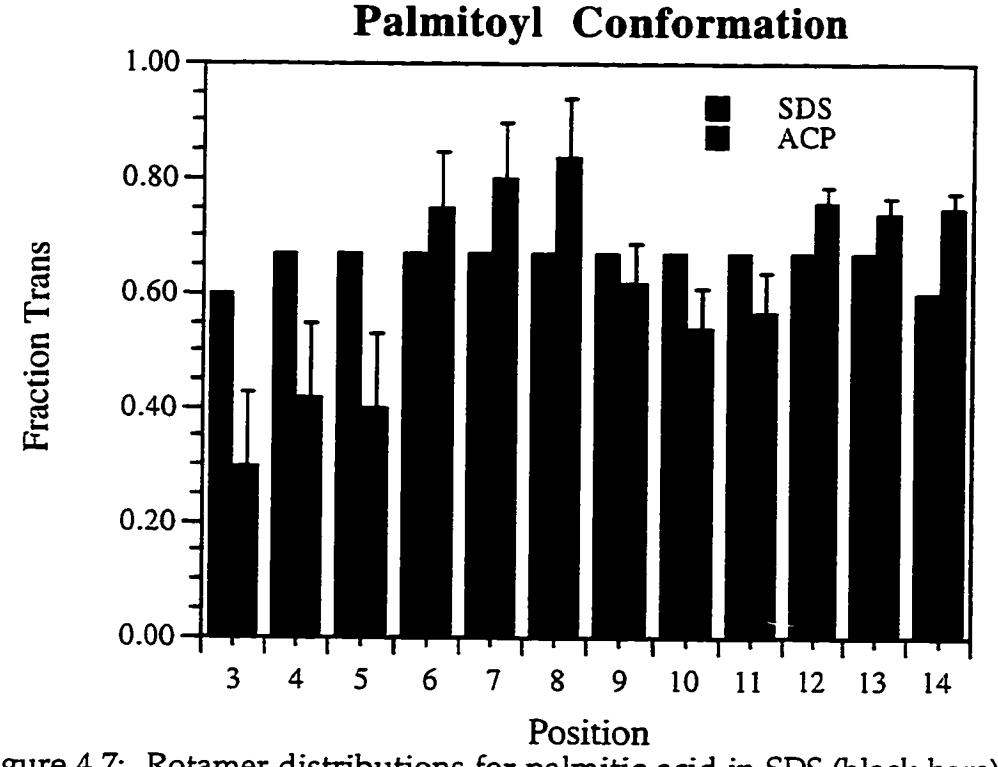

Figure 4.7: Rotamer distributions for palmitic acid in SDS (black bars) and bound to ACP (gray bars). Error bars are shown on the calculated values for the ACP bound form and are based upon an uncertainty of 0.2 ppm in the measured carbon-13 chemical shift. Position 3 represents the dihedral angle involving carbons 1-2-3-4, and so on.

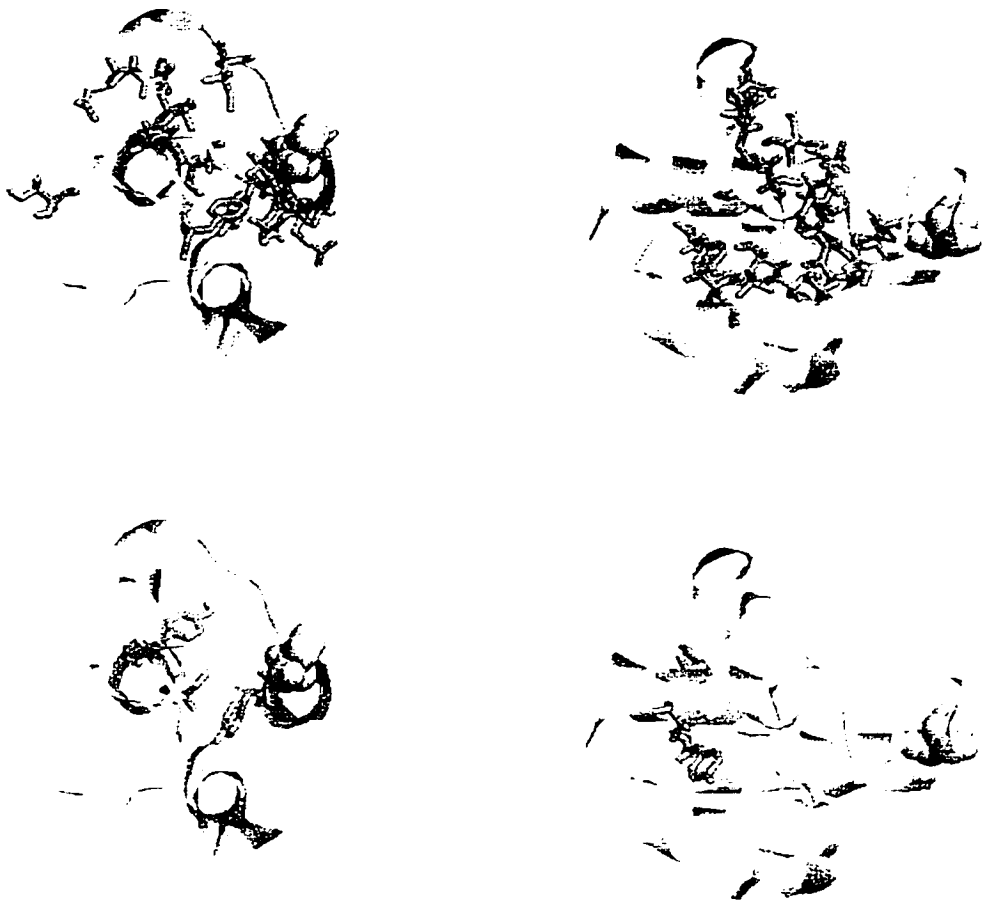

Figure 4.8 Views of contacts seen in octanoyl-ACP (top, Jones, 1991) and palmitoyl-ACP (bottom). At left is a short axis view of the helices with helix II at right and helix I at bottom. In the view at right, helix III is on top with II center and I at bottom. In all views, serine-36 is shown in a space-filling view, and residues which showed acyl chain contacts are shown as thick wireframe.

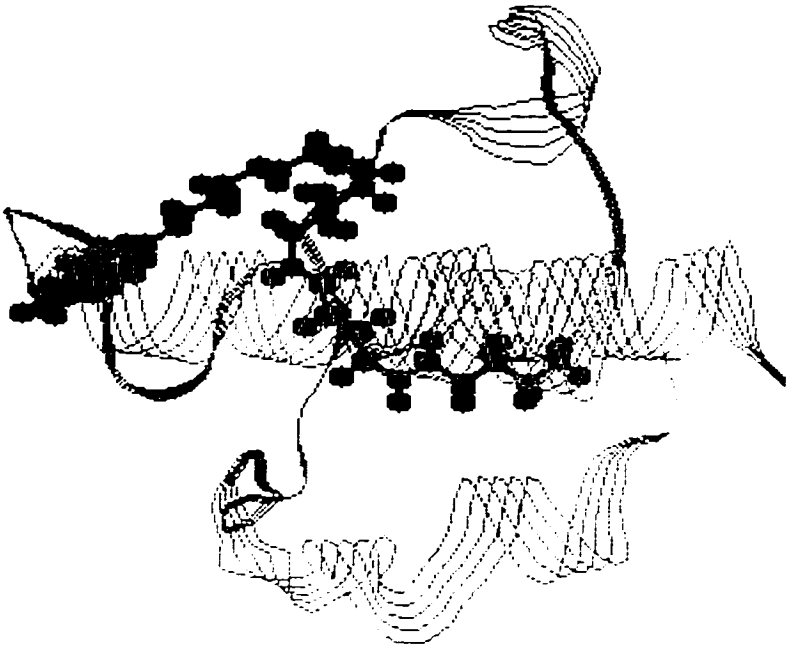

Figure 4.9: Model of palmitoyl-ACP showing acyl chain and prosthetic group looped into solution with methyl terminus contacting aromatic pocket. The positions which, on average, have a higher percentage of gauche bonds in the chemical shift data are shown in bent conformation. This model represents the average of a large number of rapidly exchanging acyl chain conformations.

Table IV-A
Chemical Shift Assignments andChanges for Palmitic Acid in SDS and ACP Samples

Position	SDS ^{1}H	ACP ^{1}H	Change	SDS ^{13}C	ACP ^{13}C	Change
2	2.23	2.49, 2.41	+0.26, 0.18	38.6	46.4	+7.8
3	1.58	1.38	-0.20	28.4	27.8	-0.6
4	1.32	1.05, 0.97	-0.27, 0.35	32.5	30.9	-1.6
5	1.32	0.90	-0.42	32.9	31.2	-1.7
6	1.32	0.86	-0.46	32.5	31.3	-1.2
7	1.30	0.90	-0.40	33.1	32.1	-1.0
8	1.30	0.92	-0.38	32.8	32.6	-0.2
9	1.29	0.93	-0.36	33.0	32.6	-0.4
10	1.28	0.94	-0.34	32.6	32.7	+0.1
11	1.28	1.04	-0.24	32.6	32.7	+0.1
12	1.28	1.04	-0.24	33.2	32.6	-0.6
13	1.26	1.12	-0.14	32.1	32.3	+0.2
14	1.25	1.14, 1.00	-0.11, 0.25	34.6	35.0	+0.4
15	1.27	1.12	-0.15	25.2	25.5	+0.3
16	0.85	0.75	-0.1	16.3	17.1	+0.9

Table IV-B
Double-Quantum Shift Calculations for Palmitic Acid Bound to ACP

Position	SQ ^{13}C	DQ ^{13}C 31.8/32.3	Calc. DQ
2	46.4	*-2.4f(7.6u)*	*7.6*
3	27.8	-5.1	-4.9
4	30.9	*-2.5*	*-2.5*
5	31.2	-0.9	-1.1
6	31.3	*-0.9*	*-1.2*
7	32.1	1.2	1.1
8	32.6	*0.7*	*0.6*
9	32.6	2.3	1.7
10	32.7	*1.0*	*0.8*
11	32.7	1.8	1.7
12	32.6	*0.3*	*0.3*
13	32.3	3.6	3.7
14	35.0	*1.8f (-4.2u)*	*-4.1*
15	25.5	-1.1f (-21.1u)	-21.1
16	17.1		

Table IV-C
Conformationally-Induced Chemical Shift Changes for Palmitic Acid Bound to ACP

Position	^{1}H Change	^{13}C Change	Corrected ^{13}C Change	Conformational shift	Change in trans fraction
2	+0.26, 0.18	+7.8			
3	-0.20	-0.6			
4	-0.27, 0.35	-1.6	-1.29	+0.41	0.068±0.17
5	-0.42	-1.7	-1.28	-1.70	-0.283±0.13
6	-0.46	-1.2	-0.74	-1.51	-0.252±0.13
7	-0.40	-1.0	-0.60	-1.70	-0.283±0.13
8	-0.38	-0.2	+0.18	+0.42	+0.070±0.10
9	-0.36	-0.4	-0.04	+0.77	+0.128±0.10
10	-0.34	+0.1	+0.44	+1.10	+0.183±0.10
11	-0.24	+0.1	+0.34	-0.24	-0.040±0.067
12	-0.24	-0.6	-0.36	-0.81	-0.135±0.067
13	-0.14	+0.2	+0.34	-0.66	-0.110±0.067
14	-0.11, 0.25	+0.4	+0.58	+0.58	+0.097±0.033
15	-0.15	+0.3	+0.45	+0.45	+0.075±0.033
16	-0.1	+0.9	+1.0	+1.0	+0.167±0.033

Table IV-D
Acyl Chain-Protein NOE's Observed in 100 ms HSQC-NOESY of Palmitoyl-ACP

^{1}H ppm	^{13}C ppm	^{1}H assignment	^{13}C assignment
0.037	16.956	Ile72m	C16
6.421	16.973	Tyr71e	C16
6.804	17.017	Tyr71d	C16
3.384	17.022	ø[1]	C16
3.794	17.025	ø	C16
2.412	17.027	ø	C16
1.170	17.028	H15	C16
0.748	17.031	H16	C16
3.453	17.035	ø	C16
1.122	17.035	H15	C16
7.559	17.080	PHe-50d	C16
6.423	25.412	Tyr71e	C15
1.124	25.453	H15	C15
6.805	25.461	Tyr71d	C15
1.008	25.499	H14b	C15
3.792	25.502	ø	C15
3.880	27.570	ø	C3
4.018	27.579	ø	C3
2.400	27.584	H2b	C3
1.374	27.597	H3	C3
2.489	27.657	H2a	C3
2.485	30.795	H2a	C4
1.053	30.879	H4	C4
2.622	30.962	ø	C4

^{1}H ppm	^{13}C ppm	^{1}H assignment	^{13}C assignment
1.371	30.962	ø	C4
4.021	31.046	ø	C4
2.414	31.129	H2b	C4
3.889	31.296	ø	C4
3.598	31.296	ø	C4
6.422	34.936	Tyr71e	C14
1.003	34.943	H14b	C14
1.136	34.947	H14a	C14
3.794	35.027	ø	C14
1.381	46.421	H3	C2
2.486	46.439	H2a	C2
2.401	46.439	H2b	C2
4.019	46.464	ø	C2
3.881	46.475	ø	C2

[1]ø indicates peak is not assigned in proton dimension. .

Chapter 5: Conclusions

5.1 Summary of Work

In this work we have described an approach to the study of acyl chain-protein interactions which makes use of pairwise ^{13}C labeling and heteronuclear NMR spectroscopy. Specific heteronuclear techniques used here include proton-detected carbon double-quantum spectroscopy and carbon-filtered NOESY experiments. This approach has proven effective in overcoming many difficulties inherent in NMR spectroscopy of fatty acids, including chemical shift degeneracy and background supression. Analysis of measured chemical shifts has provided insight into the conformation of bound acyl chains. Carbon-13 filtered NOE's proved to be a useful method for the determination of acyl chain contacts in protein-bound forms.

Two illustrative applications have been made. In the case of rat adipocyte lipid binding protein insight into the ligand-protein interactions which exist in solution has been gained. The fatty acid appears to be bound in an ionized form, and the preferred bound conformation for the acyl chain seen in crystal structures of FABP's appear to be preserved in solution.

In the case of *E. coli* acyl carrier protein a model for acyl chain exposure to enzymes of the fatty acid synthetase system has evolved. Chemical shift conformational analysis reveals several bends in a bound palmitoyl chain, while heteronuclear filtered NOE's suggest that contacts between the acyl

chain methyl terminus and several aromatic side chains of ACP are maintained. This requires that the thioester linkage loop out into solution as the chain is elongated, possibly increasing accessibility to enzyme processing.

It is interesting to compare the studies done on ALBP and ACP. Even though these systems are quite different in function and structure, the data presented here have given insight into the structure and mode of binding in both cases. Carbon-13 chemical shift data were able to give insight into the conformation of the acyl chain. In each case, the chain had specific regions which showed a tendency to bend in discrete regions. In the case of ALBP, correlation with crystallographic data suggests that these bends may be induced by steric interference from water molecules which share the binding cavity with the ligand (Xu, et al., 1993). The bound conformations for palmitoyl-ACP appear to be produced by interactions of the acyl chain with specific hydrophobic residues, as shown by this and previous studies (Jones, 1991). The ligand is not covalently bound in ALBP, but this study has shown that there is an ionic interactions between the negatively charged fatty acid carbonyl and a positively charged residue, probably arginine (Xu, et al., 1991). With ACP, the ligand is covalently attached to a phosphopantetheine prosthetic group. In both systems there is an interaction between the acyl chain and a chiral binding site on the protein with results in the resolution of diastereotopic proton pairs at the C2 position. This effect extends to several other positions in palmitoyl-ACP.

5.2 Future Directions

Studies of ALBP were limited by the poor solubility of the protein-fatty acid complex. This made any attempt at a full solution structure unfeasible. However, these methods could be applied to other FABP's which are more amenable to a complete NMR analysis, such as those for which a solution structure of the apo form is known (Lassen, et al., 1993).

The acyl chain binding site of *E. coli* ACP is now fairly well characterized. However, it would be useful to support the suggested looped-out model for long chains with other data. Two sources of NMR data which would make use of the pairwise ^{13}C labeling are scalar coupling and spin relaxation measurements. In principle, the double labeling could allow separation of ^{1}H-^{13}C and ^{13}C-^{13}C contributions to relaxation to give a more complete definition of acyl chain motion. Variations in relaxation properties as a function of position may suggest increased mobility for the looped-out portion. J-coupling constants, including large one-bond couplings, reflect average torsion angles (Carmichael, et al., 1993). The time averaging of these is different from NOE's or chemical shift, so these data would be complementary to results presented here. Another application for these acyl-ACP probes would be in the study of interactions directly with synthetic enzymes. These probes would be especially useful in studying large

complexes including ACP because of the ability to do efficient spectroscopic filtering.

The methodology employed here shows promise for the observation of discrete resonances of interest in other large protein complexes; the data on chemical shift changes are particularly easy to obtain. As noted in the introductory chapter, the acyl chains in the endotoxic lipid A component of the *E. coli* cell wall are labeled in pairwise fashion in the cultures prepared in this study and could be used in a study of immune system interactions with endotoxin (Munford, et al., 1992).

References

Anderson, M. S., Bulawa, C. E., & Raetz, C. R. H. (1985) *J. Biol. Chem. 260,* 15536-15541.

Bailie, A.G., Wilson, T.D., O'Brien, R.K., Beebe, J.M., Stuart, J.D., McCosh-Lilie, E.J., & Hill, D.W. (1982) *J. Chromatographic Science 20,* 466.

Banaszak, L., Winter, N., Xu, Z., Bernlohr, D.A., Cowan, S. & Jones, T.A. (1994) *Advances in Protein Chemistry 45,* 89-151.

Batchelor, J.G., Cushley, R.J., & Prestegard, J.H. (1974) *J. Organic Chem. 39,* 1698-1705.

Brozek, K.A., & Raetz, C.R. (1990) *J. Biol. Chem. 265,* 15410-15417.

Buelt, M.K., Shekels, L.L., Jarvis, B.W., & Bernlohr, D.A. (1991) *J. Biol. Chem. 266,* 12266-12271.

Carmichael, I., Chipman, D.M., Poklasek, C.A., & Serianni, A.S. (1993) *J. Am. Chem . Soc. 115,* 10863-10870.

Cheney, B.V., & Grant, D.M. (1967) *J. Am. Chem. Soc. 89,* 5319-5327.

Chung, J., Tolman, J.R., Howard, K.P, & Prestegard, J.H. (1993) *J. Magnetic Resonance B 102,* 137.

Cistola, D.P., Walsh, M.T., Corey, R.P., Hamilton, J.A. & Brecher, P. (1988) *Biochemistry 27,* 711-717.

Cistola, D.P., Sacchetini, J.C., Banaszak, L.J., Walsh, M.T., & Gordon, J.I. (1989) *J. Biol. Chem. 264,* 2700-2710.

Clarke, S.D., & Armstrong, M.K. (1989) *FASEB J. 3,* 2480-2487.

Cronan, J.E. Jr. (1982) *J. Biol. Chem. 257,* 5013-5017.

Cronan, J.E. Jr. & Batchelor, J.G. (1973) *Chem. Phys. Lipids 11,* 196-202.

Cronan, J.E. Jr. & Klages, A.L. (1981) *Proc. Natl. Acad. Sci. USA 78,* 5440-5444.

Cronan, J.E. Jr., Nunn, W.D., & Batchelor, J.G. (1974) *Biochim. Biophys. Acta 348,* 63-75.

de Dios, A.C., Pearson, J.G., & Oldfield, E. (1993) *J. Am. Chem. Soc. 115,* 9768-9773.

Ernst, R.R., Bodenhausen, G., & Wokaun, A. (1987)*Principles of Nuclear Magnetic Resonance in One and Two Dimensions,* p. 193. Oxford Univ. Press, New York.

Glatz, J.F.C., Vork. M.M., Cistola, D.P., & van der Vusse, G.J. (1993) *Prostaglandins; Leukotrienes, and Essential Fatty Acids 48,* 33-41.

Guerra, D.J., & Browse, J.A. (1990) *Arch. Biochem. Biophys. 280,* 336-345.

Hill, R. B., MacKenzie, K. R., Flanagan, J. M., Cronan, J. E. Jr., & Prestegard, J. H. (1995) *Protein Expression and Purification 6,* 394-400.

Holak, T. A., & Prestegard, J. H. (1986) *Biochemistry 25,* 5766-5772.

Holak, T. A., Kearsley, S. K. , Kim, Y., & Prestegard, J. H. (1988) *Biochemistry 27,* 6135-6140.

Issartel, J.-P., Koronakis, V., & Hughes, C. (1991) *Nature 351,* 759-761.

Jackowski, S., Hsu, L, & Rock, C. O. (1992) *Meth. Enzymology 209,* 111-117.

Jones, P.-J. (1991) *Structural Studies of Acyl-Acyl Carrier Protein,* Ph.D. Thesis. Yale University, New Haven, CT.

Jones, P.-J., Cioffi, E. A., & Prestegard, J.H. (1987a) *J. Biol. Chem. 262,* 8963-8965.

Jones, P.-J., Holak, T. A., & Prestegard, J.H. (1987b) *Biochemistry 26,* 3493-3499.

Jorgenson, W.L., Madura, J.D., & Swenson, C.J. (1984) *J. Am. Chem. Soc. 106,* 6638-6646.

Kay, L.E., Keifer, D., & Saarinene, T. (1992) *J. Am. Chem. Soc. 114,* 10663-10665.

Kim, Y. & Prestegard, J.H. (1989) *Biochemistry 28,* 8792-8797.

Law, J.H. (1971) *Acc. Chem. Res. 4,* 199-203.

LaLonde, J.M., Bernlohr, D.A., & Banaszak, L.J. (1994) *Biochemistry 33,* 4885-4895.

Lassen, D., Lücke, C. Kromminga, A., Lezius, A. Spener, F. & Rüterjans, H. (1993) *Molecular Cellular Biochem. 123,* 15-22.

Matarese, V., & Bernlohr, D.A. (1988) *J. Biol. Chem 263,* 14544-14551.

Mayo, K. H. & Prestegard, J. H. (1985) *Biochemistry 24,* 7834-7838.

Munford, R.S., Cronan, J.E. Jr., & Rick, P. D. (1992) *J. Immunological Methods 148,* 115-120.

Norris, A.W., Rong, D., d'Avignon, D.A., Rosenberger, M., Tasaki, K., & Li, E. (1995) *Biochemistry 34,* 15564-15573.

Norwood, T.J. (1992) *Prog. NMR Spectroscopy 24,* 295-375.

Ohlrogge J.B., Shine W.E., & Stumpf P.K. (1978) *Arch Biochem Biophys 189,* 382-91.

Pouchert, C.J. & Behnke, J. (1993) *The Aldrich Library of* ^{13}C *and* ^{1}H *FTNMR Spectra,* pp. 752, 907. Aldrich Chemical Co., Milwaukee, WI.

Pugh, E.L., & Kates, M. (1984) *Lipids 19,* 359-362.

Rance, M., Wright, P.E., Messerle, B.A., & Field, L.D. (1987) *J. Am. Chem. Soc. 109,* 1591-1593.

Richieri, G.V., Ogata, R.T., & Kleinfeld, A.M. (1994) *J. Biol. Chem. 269,* 23918-23930.

Rock, C. O., & Cronan, J. E. (1981) *Meth. Enzymology 71,* 163-168.

Rock, C. O., & Garwin, J. L. (1979) *J. Biol. Chem. 254,* 7123-7128.

Schaller, W. & Robertson, A.D. (1995) *Biochemistry 34,* 4714-4721.

Schumann, R. R., Leong, S. R., Flaggs, G. W., Gray, P. W., Wright, S. D., Mathison, J. C., Tobias, P. S., & Ulevitch, R. J. (1990) *Science 249,* 1429-1431.

Slabas, A. R., & Fawcett, T. (1992) *Plant Molecular Biology 19,* 169-191.

Spencer, A.K., Greenspan, A.D., & Cronan, J.E. Jr. (1978) *J. Biol. Chem. 253,* 5922-5926.

Spera, S. & Bax, A. (1991) *J. Am. Chem. Soc. 113,* 5490-5492.

Stanley, P., Packman, L.C., Koronakis, V., & Hughes, C. (1994) *Science 266,* 1992-1996.

Tolman, J.R., Chung, J., & Prestegard, J.H. (1992) *J. Magnetic Resonance 98,* 462-467.

Veerkamp, J. H., Peeters, R. A., & Maatman, R. G. H. J. (1991) *Biochim. Biophys. Acta 1081,* 1-24.

Voelker, T.A., Worrell, A.C., Anderson, L., Bleibaum, J., Fan, C., Hawkins, D.J., Radke, S.E., & Davies, H.M. (1992) *Science 257,* 72-74.

Ways, P. & Hanahan, D.J. (1964) *J. Lipid Research 5,* 318-328.

Wishart, D.S. & Sykes, B.D. (1994) *J. Biomolecular NMR 4,* 171-180.

Wishart, D.S., Bigam, C.G., Yao, J., Abildgard, F., Dyson, H.J., Oldfield, E., Markley, J.L., & Sykes, B.D. (1995) *J. Biomolecular NMR 6,* 135-140.

Xu, Z., Bernlohr, D.A., & Banaszak, L.J. (1993) *J. Biol. Chem. 268,* 7874-7884.

Xu, Z., Buelt, M.K., Banaszak, L.J., & Bernlohr, D.A. (1991) *J. Biol. Chem. 266,* 14367-14370.